Geochemistry Geophysics Geosystems G3
AN ELECTRONIC JOURNAL OF THE EARTH SCIENCES
Published by AGU and the Geochemical Society

Article
Volume 11, Number 3
27 March 2010
Q03016, doi:10.1029/2009GC002869
ISSN: 1525-2027

Continental bedrock and riverine fluxes of strontium and neodymium isotopes to the oceans

Bernhard Peucker-Ehrenbrink
Department of Marine Chemistry and Geochemistry, Woods Hole Oceanographic Institution, 360 Woods Hole Road, MS 25, Woods Hole, Massachusetts 02543-1543, USA (bpeucker@whoi.edu)

Laboratoire d'Etudes en Géophysique et Océanographie Spatiale, UPS, CNRS, CNES, IRD, Observatoire Midi-Pyrénées, 14 avenue E. Belin, F-31400 Toulouse, France

Mark W. Miller
BenchmarkGIS Services, Chapel Hill, North Carolina 27516, USA

Thomas Arsouze and Catherine Jeandel
Laboratoire d'Etudes en Géophysique et Océanographie Spatiale, UPS, CNRS, CNES, IRD, Observatoire Midi-Pyrénées, 14 avenue E. Belin, F-31400 Toulouse, France

[1] Realistic models of past climate and ocean chemistry depend on reconstructions of the Earth's surface environments in the geologic past. Among the critical parameters is the geologic makeup of continental drainage. Here we show, for the present, that the isotope composition of dissolved strontium in rivers increases linearly with the age of bedrock in drainage basins, with the notable exception of the drainage area of Arabia, India, and Southeast Asia that is affected by unusually radiogenic dissolved Sr from the Himalaya. We also demonstrate that the neodymium isotope compositions of suspended matter in rivers as well as clastic sediments deposited along the ocean margins decrease linearly with the bedrock ages of river drainage basins and large-scale continental drainage regions, as determined from digital geologic maps. These correlations are used to calculate the present-day input of dissolved Sr (4.7×10^{10} mol yr^{-1}, $^{87}Sr/^{86}Sr$ of ~0.7111) and particulate Nd isotopes (ε_{Nd} of approximately -7.3 ± 2.2) to the oceans. The fact that the regionally averaged ε_{Nd} of the global detrital input to the global coastal ocean is identical to globally averaged seawater (ε_{Nd} of -7.2 ± 0.5) lends credence to the importance of "boundary exchange" for the Nd isotope composition of water masses. Regional biases in source areas of detrital matter and runoff are reflected by the observation that the average age of global bedrock, weighted according to the riverine suspended sediment flux, is significantly younger (~336 Myr) than the age of global bedrock weighted according to water discharge (394 Myr), which is younger than the average bedrock age of the nonglaciated, exorheic portions of the continents (453 Myr). The observation that the bedrock age weighted according to Sr flux is younger (339 Myr) than that weighted according to water flux reflects the disproportionate contribution from young sedimentary and volcanic rocks to the dissolved Sr load. Neither the isotope composition of the dissolved nor the particulate continental inputs to the ocean provide unbiased perspectives of the lithologic makeup of the Earth's surface. Temporal changes in bedrock geology as well as the shifting focal points of physical erosion and water discharge will undoubtedly have exerted strong controls on temporal and spatial changes in the isotope chemistry of past global runoff and thus seawater.

Components: 14,799 words, 7 figures, 5 tables.

Keywords: seawater; river; strontium; neodymium; isotope; continental runoff.

Index Terms: 1030 Geochemistry: Geochemical cycles (0330); 1040 Geochemistry: Radiogenic isotope geochemistry; 1022 Geochemistry: Composition of the hydrosphere.

Received 22 September 2009; **Revised** 4 January 2010; **Accepted** 13 January 2010; **Published** 27 March 2010.

Peucker-Ehrenbrink, B., M. W. Miller, T. Arsouze, and C. Jeandel (2010), Continental bedrock and riverine fluxes of strontium and neodymium isotopes to the oceans, *Geochem. Geophys. Geosyst.*, *11*, Q03016, doi:10.1029/2009GC002869.

1. Introduction

[2] Earth's differentiation has created two near-surface reservoirs with contrasting geochemical properties [e.g., *Hofmann*, 1988]. The depleted mantle forms oceanic crust that, owing to its low Rb/Sr and elevated Sm/Nd relative to the Bulk Silicate Earth (BSE), has relatively uniform unradiogenic $^{87}Sr/^{86}Sr$ (~0.7025) and radiogenic $^{143}Nd/^{144}Nd$ (i.e., high ε_{Nd} values of ~+10). In contrast, the geochemically extremely diverse continental crust with, on average, elevated Rb/Sr and low Sm/Nd, has radiogenic $^{87}Sr/^{86}Sr$ (~0.72) and unradiogenic $^{143}Nd/^{144}Nd$ (i.e., low ε_{Nd} values of approximately −10). The interactions of the hydrosphere with these reservoirs determine the Sr and Nd isotope compositions of seawater.

[3] The marine records of Nd and Sr isotopes complement each other; marine Nd is almost exclusively of continental origin, and the great majority of continental Nd is transported to the coastal ocean bound to particles [*Tachikawa et al.*, 2003]. The particle-reactive properties of Nd shorten its residence time in seawater, cause strong regional variations in the present-day distribution of Nd isotopes, and make this isotope system responsive to changes in input or output fluxes. These properties make reconstructions of spatial and temporal variations in the geologic past onerous [e.g., *Keto and Jacobsen*, 1988]. The soluble nature of Sr, in contrast, causes a well mixed ocean reservoir with a long residence time of Sr. This reservoir, though dominated by continental inputs, also responds to changes in the input from submarine hydrothermal sources in the oceanic crust [*Albarede et al.*, 1980]. Earlier work has shown that the inputs of Sr and Nd isotopes from the continents vary systematically as functions of the model ages [*Goldstein and Jacobsen*, 1987, 1988] as well as the isotope compositions of the source terrains of detrital [*Jeandel et al.*, 2007; *Arsouze*, 2008] and dissolved matter. We have known qualitatively for decades that [*Goldstein and Jacobsen*, 1987, p. 269] "the isotopic composition of both Sr and Nd in rivers is primarily controlled by the age of the rocks in a drainage basin."

[4] Here, we quantitatively explore the relationship between bedrock ages (i.e., eruption ages of volcanic rocks, depositional ages of sedimentary rocks, emplacement ages of plutonic rocks and the last high-grade metamorphic overprint of metamorphic rocks) of continental drainage basins and Sr and Nd isotope compositions of continental sources. This approach makes use of digital maps of bedrock geology to estimate the Sr and Nd isotope composition of riverine dissolved and suspended particulate matter, respectively. In contrast to maps of model ages or isotope composition, digital maps of bedrock geology are available at various spatial and temporal resolutions for the entire nonglaciated land surface [e.g., *Peucker-Ehrenbrink and Miller*, 2007]. In addition, paleoreconstructions of bedrock geology have been attempted, albeit at much lower spatial and temporal resolution [*Ronov*, 1989; *Bluth and Kump*, 1991]. This opens up the prospect of converting such maps into maps of Sr and Nd isotope compositions of continental inputs to the ocean in the geologic past. Here we focus on the present-day inputs. We base our bedrock analyses on a range of spatial scales, from tributary basins within the Fraser and Mississippi River basins for which we have the most detailed data, to a global analysis of large-scale continental drainage regions [*Graham et al.*, 1999, 2000; *Peucker-Ehrenbrink and Miller*, 2007; *Peucker-Ehrenbrink*, 2009]. This data is then used in conjunction with a compilation of data on the present-day supply of riverine dissolved $^{87}Sr/^{86}Sr$ and particulate ε_{Nd} to the oceans in an attempt to establish relationships between the age structure of drainage areas and the isotope compositions of present-day seawater.

2. Data and Methods

[5] We used a variety of data and methods to gain insights into the relationship between the Sr and Nd isotope composition of continental runoff and the lithologic makeup and age structure of continental

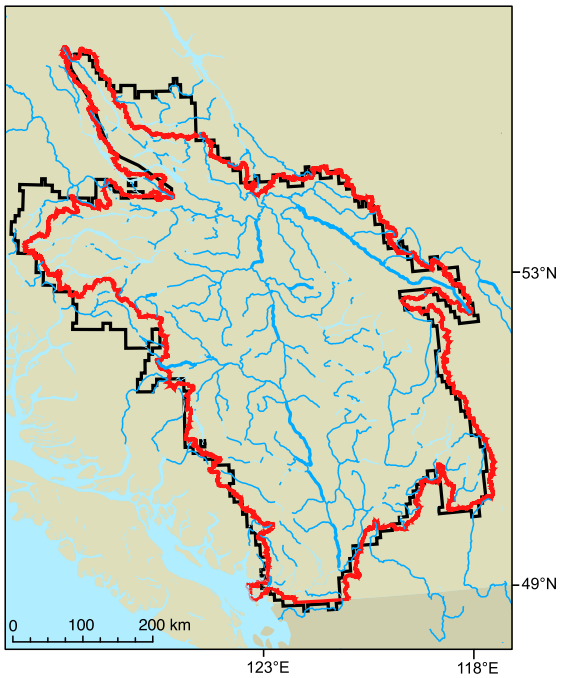

Figure 1. Outlines of the Fraser River basin according to digital maps provided by the British Columbia Fisheries Service, B.C., Canada (shown in red), and the World Resources Institute, Washington, D. C. [*Revenga et al.*, 1998], shown in black. The drainage network of the Fraser River and its tributaries is depicted in blue. Note that the B.C. data set neglects small areas in NW Washington. Major discrepancies between both models exist in the northern part of the basin that is dominated by peneplain areas. We use the B.C. data set because it also provides outlines of the subdrainage basins within the Fraser River basin. Note that the diversion of water to the Pacific Ocean by the Nechako dam has not been taken into account by either model.

bedrock. ENRI's ArcInfo® Geographic Information System was used to quantify bedrock geology of individual river basins, tributary basins and large-scale drainage regions. The digital geologic maps of Alaska, Canada, the conterminous United States, East and Southeast Asia, as well as the world used in this study are identical to those evaluated by *Peucker-Ehrenbrink and Miller* [2002, 2003, 2004, 2007]. Digital polygons of river drainage basins investigated here are primarily based on data from the World Resources Center in Washington, D. C. [*Revenga et al.*, 1998]. For the Fraser River basin and its subdrainage basins we also use digital polygons provided by the British Columbia Fisheries Service. The accuracy of the outlines of drainage basins depends on the spatial scale of the digital maps as well as the digital elevation and hydrologic data and models used to route water from source to sink. The outlines of the Fraser river basin, for example, are defined slightly differently by the British Columbia Fisheries Service and the World Resources Center [*Revenga et al.*, 1998] and exemplify the uncertainties involved in the quantitative analysis of bedrock geology of drainage basin (Figure 1). In order to achieve global coverage we also use the digital outlines of the large-scale drainage regions defined by *Graham et al.* [1999, 2000]. The continental bedrock geology (lithology and bedrock age) of these regions has been evaluated by *Peucker-Ehrenbrink and Miller* [2007]. We use this data in conjunction with the Land2Sea database [*Peucker-Ehrenbrink*, 2009] on river basin sizes (in km^2, 1527 rivers), annual water discharges (in $km^3\ yr^{-1}$, 1273 rivers) and suspended sediment fluxes (in $Mt\ yr^{-1}$, 599 rivers), as well as the isotope composition of dissolved (Sr, n = 193 (see Data Set S1)) and suspended particulate (Nd, n = 79 [*Jeandel et al.*, 2007; *Arsouze*, 2008]) matter of rivers to calculate regional fluxes of Sr and Nd isotopes to the coastal ocean.[1]

[6] The isotope data were generated after the onset of significant anthropogenic modification of river basins and may not reflect preanthropogenic conditions. For instance, the global number of dams has increased steeply between 1950 and 1980 [*Chao et al.*, 2008], trapping significant amounts of sediment. $^{143}Nd/^{144}Nd$ of suspended particulates sampled downstream of dams may therefore no longer reflect the integrated $^{143}Nd/^{144}Nd$ of the entire drainage basin. Similarly, water consumption for irrigation and industry, increased evapotranspiration and soil erosion have altered the flux of dissolved constituents from intensely utilized river basins such as the Huanghe [*Wang et al.*, 2006, 2007] and the Colorado River [*Cohen et al.*, 2001] to the coastal ocean. Finally, sampling locations do not necessarily coincide with the terminus of the tidal influence and thus often do not reflect the chemical signature of the entire drainage basin. For instance, Sr isotope values for the Amazon at Obidos do not include the major downstream tributaries of the Rio Xingu and Rio Tapajos. Their contributions have to be added to this Sr isotope balance in proportion to their Sr concentration and water flux. We discuss potential ramifications of these biases for the global budgets in section 3.6.

[7] Throughout this paper we use mean bedrock ages that have been linearly interpolated between known age boundaries for all maps with spatial resolutions higher than 1:5,000,000 [*Peucker-Ehrenbrink and*

[1] Auxiliary materials are available at ftp://ftp.agu.org/apend/gc/2009gc002869.

Table 1. Global Assessment of the Average Nd Isotope Composition of Modern Seawater[a]

Ocean Basin	Volume (m^3)	Fraction (%)	Analyses (n)	Average ε_{Nd}	±1 SD
Atlantic	2.57 E+17	19.9	272	−12.2	0.3
Mediterranean	3.64 E+15	0.28	73	−8.0	0.2
Austral[b]	3.32 E+17	25.6	33	−8.8	0.7
Indian	1.63 E+17	12.5	72	−6.6	0.4
Pacific	5.41 E+17	41.7	158	−4.1[c]	0.4
Global Ocean	1.30 E+18	100.0	608	−7.2	0.5

[a]Based on data compiled by Francois Lacan and Kazuyo Tachikawa, May 2006 (http://www.legos.obs-mip.fr/fr/equipes/geomar/results/database_may06.xls).
[b]Austral Ocean includes the area south of South Africa.
[c]This value is biased toward the radiogenic North Pacific.

Miller, 2002, 2003], i.e., for all individual river basins. The global bedrock map that has been used to characterize the 19 large-scale drainage regions, however, has a much lower temporal and spatial resolution (1:20,000,000 [*Commission for the Geologic Map of the World*, 2000]). At low temporal resolution mean bedrock ages of lithologies with lognormal area-age distributions (volcanic rocks, sedimentary rocks) are more accurately represented by an exponential rather than a linear age model (see *Peucker-Ehrenbrink and Miller* [2007] for a more detailed discussion). Mean bedrock ages of the large-scale drainage regions are therefore based on an exponential age model for volcanic and sedimentary rocks, and linear age models for endogenous (plutonic and metamorphic rocks). Ages of various bedrock units are weighted by area only, and no adjustments have been made to account for weatherability of various lithologies, temperature, or spatial variability in runoff and erosion.

[8] The global average Nd isotope composition of seawater was computed using the database compiled by Francois Lacan and Kazuyo Tachikawa (http://www.legos.obs-mip.fr/fr/equipes/geomar/results/database_may06.xls) from 26 original data sources [*Amakawa et al.*, 2000, 2004a, 2004b; *Bertram and Elderfield*, 1993; *Dahlqvist et al.*, 2005; *Henry et al.*, 1994; *Jeandel*, 1993; *Jeandel et al.*, 1998; *Lacan and Jeandel*, 2001, 2004a, 2004b, 2004c, 2005a, 2005b; *Piepgras and Jacobsen*, 1988; *Piepgras and Wasserburg*, 1980, 1982, 1983, 1987; *Piepgras et al.*, 1979; *Shimizu et al.*, 1994; *Spivack and Wasserburg*, 1988; *Stordal and Wasserburg*, 1986; *Tachikawa et al.*, 1999, 2004; *Vance et al.*, 2004]. The more than 600 seawater analyses have been grouped into six large ocean basins (see Table 1) [*Arsouze*, 2008], averaged and weighted according to the water volume of the respective basin. No attempts have been made to correct for variations in Nd concentration or isotope composition with water depth, and the data have not been weighted according to location within each basin.

[9] Statistical parameters calculated for various linear regressions discussed below are summarized in Table 2. These parameters include the Pearson correlation coefficient (r), zero-bedrock age intercepts in $^{87}Sr/^{86}Sr$, ε_{Nd} and specific Sr flux with their respective 95% confidence intervals (CI), and slopes of the linear regressions with their respective 95% confidence intervals.

3. Results: Bedrock Ages, Lithology, and Isotope Systematics of River Drainage Basins, Large-Scale Drainage Regions, and Ocean Margin Sediments

3.1. Fraser and Mississippi River Basins

[10] The Fraser River is a medium-sized river basin (248,035 km^3 [*Revenga et al.*, 1998]; 112 $km^3\ yr^{-1}$ water discharge [*Milliman et al.*, 1995]) that drains portions of the North American Cordillera and the Coast Range into the Strait of Georgia (Pacific Ocean). Its lithologically and tectonically complex drainage basin is dominated by steep hillslopes and large topographic gradients. It therefore is likely a good analog for a weathering-limited drainage basin. Precambrian and Phanerozoic sedimentary rocks dominate the Rocky Mountain Foreland Belt in the east, whereas Mesozoic and Cenozoic igneous rocks dominate the Coast Range in the west. The Fraser River is one of the more pristine larger North American rivers [*Revenga et al.*, 1998]; only three large dams block some of the large tributaries, developed areas, including one large city, cover only 13% of the basin, and 93% of the forest cover remains [*Revenga et al.*, 1998], albeit in an altered state [*Kurz et al.*, 2008].

Table 2. Pearson Correlation Coefficients, Zero-Bedrock Age Intercepts With Respective 95% Confidence Intervals, and Slopes With 95% Confidence Intervals of Various Linear Regressions[a]

Figure and Data	r	Intercept ± 95% CI	Slope ± 95% CI
Figure 4a, drainage regions (w/o EA and AIA), (n = 14)	0.832	0.7079 ± 0.0016	$6.5 \times 10^{-6} \pm 2.7 \times 10^{-6}$
Figure 4a, Fraser River system (n = 8)	0.971	0.7026 ± 0.0030	$2.9 \times 10^{-5} \pm 0.7 \times 10^{-6}$
Figure 4a, Mississippi-Nelson system (n = 5)	0.993	0.7071 ± 0.0008	$8.7 \times 10^{-6} \pm 1.9 \times 10^{-6}$
Figure 4b, margin sediments (median values, w/o Antarctica) (n = 15)	0.903	1.9 ± 4.0	−0.023 ± 0.007
Figure 4b, drainage regions (n = 12)	0.867	−2.7 ± 4.7	−0.019 ± 0.008
Figure 4b, Fraser River system (n = 8)	0.935	3.8 ± 5.3	−0.033 ± 0.013
Figure 4b, large rivers[b] (n = 9)	0.703	−9.1 ± 2.2	−0.006 ± 0.005
Figure 4b, margin sediments and drainage regions (n = 27)	0.876	−0.2 ± 2.9	−0.021 ± 0.005
Figure 5, individual river basins (n = 171)	0.758	12 ± 12	0.57 ± 0.07
Figure 5, drainage regions (n = 16)	0.467	16 ± 27	0.60 ± 0.65
Figure 6, individual river basins (n = 91)	0.609	50 ± 14	0.028 ± 0.008
Figure 6, drainage regions (n = 16)	0.380	28 ± 20	0.05 ± 0.07

[a]Zero-bedrock age intercepts are in units of $^{87}Sr/^{86}Sr$ (Figure 4a), ε_{Nd} (Figure 4b), or kg Sr km^{-2} yr^{-1} (Figures 5 and 6). CI, confidence interval; r, Pearson correlation coefficient; EA, East Africa; AIA, Arabia, India, and southeast Asia; w/o, without.
[b]Large rivers include the Chang Jiang (Yangtze), Hong (Red River), Hudson, Mackenzie, Mekong, Mississippi (with Ohio and Missouri), and Xi Jiang (Pearl).

[11] The Mississippi River dominates the North American drainage (3,202,230 km^2 [*Revenga et al.*, 1998]) and ranks sixth among the world's rivers in water discharge (529 km^3 yr^{-1} [*Milliman et al.*, 1995]). Its drainage basin is bounded by the Precambrian to Paleozoic Appalachian Highlands in the east, the denuded Precambrian Canadian Shield and a thin cover of glacial regolith in the north, and the lithologically and tectonically complex Rocky Mountain System in the west. The large Interior Plains consist of low-lying Tertiary to Cretaceous sedimentary platforms in the west and mostly Phanerozoic sediments in the east, making this basin a likely analog of a transport-limited drainage basin. More than 2000 large dams, 87 large cities, significant loss of original forest, and large proportions of developed areas reflect significant anthropogenic changes in the basin since the beginning of human settlement [*Revenga et al.*, 1998].

3.2. Bedrock Geology of the Fraser and Mississippi River Basins

[12] We have quantitatively investigated the lithology and age of bedrock in both basins and major tributary basins by overlaying digital bedrock maps [*King and Beikman*, 1974; *Wheeler et al.*, 1997] with digital outlines of drainage basins. Digital polygons of the Fraser tributary basins are those provided by the British Columbia Fisheries Service, Canada, whereas polygons of the Mississippi River basin and major tributary basins were taken from *Revenga et al.* [1998]. We have investigated the effect of map resolution on the accuracy of the bedrock data by comparing our data for the Mackenzie River basin at a scale of 1:5,000,000 with higher-resolution data (~1:100,000) of *Reeder et al.* [1972]. The excellent agreement between both data sets, shown in Table 3, indicates that spatial variations in bedrock are adequately captured by the digital maps used in this study. Ages are based on age information provided by *King and Beikman* [1974] and *Wheeler et al.* [1997], as well as the time scales of *Harland et al.* [1990] and *Lumbers and Card* [1991]. Uncertainties (1 standard deviation) of the average bedrock ages have been calculated with the linear age model with a Monte Carlo method assuming uniform age probabilities between the respective age boundaries [*Peucker-Ehrenbrink and Miller*, 2007].

[13] Bedrock area in the Fraser River basin (pie charts in Figure 2) is dominated by volcanic (42.3%), marine sedimentary (35.8%) and felsic intrusive (15.1%) rocks. The average bedrock age of the basin is 260 ± 39 Myr (1 standard deviation). Bedrock ages of tributary basins vary systematically by more than an order of magnitude, from old (Upper Fraser River basin: 742 ± 178 Myr; McGregor River basin: 668 ± 140 Myr) sedimentary tributary basins in the headwaters to tributary basins dominated by young igneous rocks in the lower reaches of the Fraser River (West Road River basin: 51 ± 11 Myr; Chilcotin River basin: 62 ± 8 Myr). It is important in this context to point out that glacial till does not significantly obscure primary bedrock boundaries in the Fraser River basin [*Levson and Giles*, 1995].

[14] Bedrock area in the Mississippi River basin (Figure 3) is dominated by marine (74.8%) and continental (19.7%) sedimentary rocks. The average bedrock age of the basin is 309 ± 12 Myr and

Table 3. Comparison of High-Resolution Analog and Lower-Resolution Digital Bedrock Data for the Mackenzie River Basin[a]

Lithology	*Reeder et al.* [1972]	This Study
Precambrian, nonmetamorphic	22.49	22.23
Stratified sediments, nonevaporitic	68.31	68.13
Evaporites	2.46	1.99
Volcanics and sediments	0.55	0.19
Volcanic rocks	0.35	0.74
Intrusive rocks	1.17	1.37
Ultramafic rocks	0.04	0.055
Metamorphic rocks	4.63	5.23

[a]High-resolution analog data are ~1:100,000 [*Reeder et al.*, 1972], and lower-resolution data are 1:5,000,000 [*Wheeler et al.*, 1997]. Numerical values are percent (%) of total basin bedrock area. Note that *Reeder et al.* [1972] used scissors to cut and weight lithologic units from geologic paper maps. Our data are based on GIS (ArcInfo) software and digital geologic maps.

varies by less than a factor of three between major tributary basins (Figure 3) (127 Myr for the Red River, 367 Myr for the Ohio River). In contrast to the Fraser River basin, the thick glacial till that covers some northern portions of the Mississippi River basin and obscures underlying bedrock is mapped as a unique bedrock unit of Quaternary age by the United States Geologic Survey [*King and Beikman*, 1974].

3.3. Bedrock Geology of Large-Scale Drainage Regions

[15] The lithologic composition and age structure of the 19 large-scale drainage regions [*Graham et al.*, 1999, 2000] have been evaluated by *Peucker-Ehrenbrink and Miller* [2007], and only a brief synthesis is given here. The area percentages of volcanic bedrock in the various nonglaciated, exorheic drainage regions we have isotope data for range from 0% (Baltic Sea) to 37.3% (western South America). Area percentages of sedimentary bedrock range from 38.0% (western South America) to 84.4% (Black Sea). Area percentages of endogenous (plutonic and metamorphic) bedrock range from 11.0% (Black Sea) to 45.3% (Hudson Bay). Average bedrock ages vary by more than one order of magnitude from 96 Myr (western South America) to 1549 Myr (Hudson Bay). Data for these large-scale drainage basins are summarized in Table 4 [*Peucker-Ehrenbrink*, 2009].

3.4. Strontium and Neodymium Isotope Systematics of the Fraser and Mississippi River Basins

[16] $^{87}Sr/^{86}Sr$ and $^{143}Nd/^{144}Nd$ data for the Fraser River and its major tributaries [*Cameron and Hattori*, 1997] as well as the Mississippi and some of its large

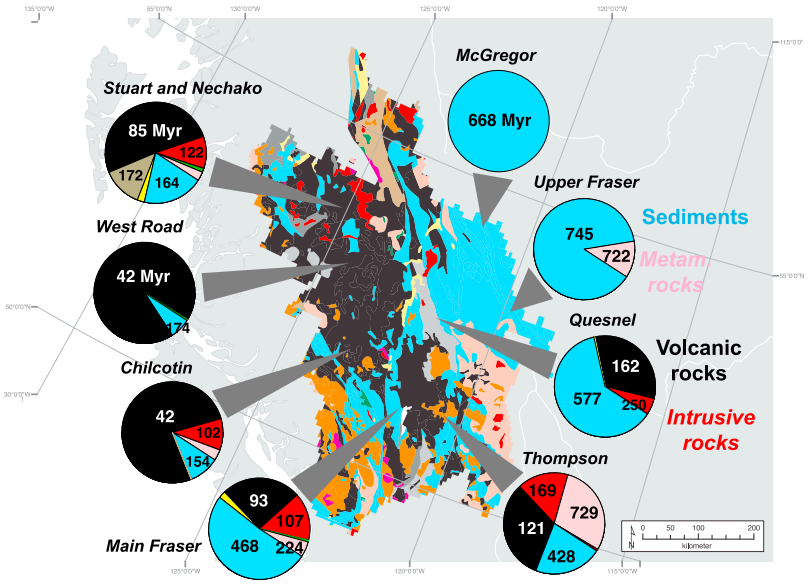

Figure 2. Bedrock geology of the Fraser River basin (geology, *Wheeler et al.* [1997]; basin outlines, British Columbia Fisheries Service, B.C., Canada). Color-coded lithologies are as follows: yellow, continental sediments; blue, marine sediments; black, mafic volcanic rocks; pink, metamorphic rocks; red, felsic intrusive rocks; orange, intermediate intrusive rocks; dark green, ultramafic rocks; light gray, felsic volcanic rocks; dark gray, intermediate volcanic rocks; brown, sediments and volcanic rocks. Pie charts summarize the lithologic composition of the major tributary basins and show the average bedrock age for the entire subdrainage basins in Myr.

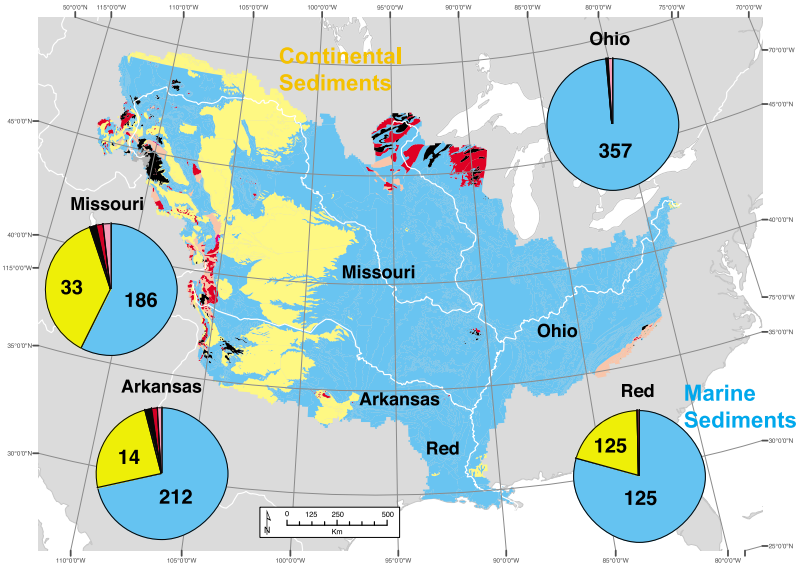

Figure 3. Bedrock geology of the Mississippi River basin (Geology, *King and Beikman* [1974]; basin outlines, WRI). Color-coded lithologies are as follows: yellow, continental sediments; blue, marine sediments; black, basic extrusive rocks; pink, metamorphic rocks; red, felsic intrusive rocks; dark green, ultramafic rocks. Pie charts summarize the lithologic composition of some of the major tributary basins and show the average bedrock age for the entire subdrainage basins in million years (Myr).

tributaries [*Goldstein and Jacobsen*, 1988] reflect the isotope compositions at medium flow and enable us to assess correlations between radiogenic isotope compositions and bedrock ages. We could not evaluate seasonal variations in the isotope compositions because such data have not been published for these rivers. There is a general lack of time series data for radiogenic isotopes that prevents proper assessment of uncertainties in estimated annual averages. The few rivers for which time series data is available (e.g., Connecticut River [*Douglas et al.*, 2002], Brahmaputra [*Rai and Singh*, 2007], Loire [*Grosbois et al.*, 2000], and Somme [*Négrel and Petelet-Giraud*, 2005]) indicate that Sr concentrations can vary by more than a factor of two, and $^{87}Sr/^{86}Sr$ can vary by several per mil.

[17] Bedrock ages of the Fraser River basin correlate linearly and positively with dissolved $^{87}Sr/^{86}Sr$ (red symbols and line in Figure 4a and Table 2) and negatively with the $^{143}Nd/^{144}Nd$ of the suspended particulate load (red symbols and line in Figure 4b and Table 2). These systematics reflect the behavior of the ^{87}Rb-^{87}Sr and ^{147}Sm-^{143}Nd parent-daughter decay systems in the Earth's mantle and crust [*Goldstein*, 1988]. The linear trends are also consistent with the observed two-component mixing between an old source with radiogenic $^{87}Sr/^{86}Sr$ and unradiogenic $^{143}Nd/^{144}Nd$, and a young source with opposite isotope characteristics [*Cameron and Hattori*, 1997]. The dissolved $^{87}Sr/^{86}Sr$ in the Mississippi River and its tributaries also correlate positively and linearly with bedrock age, but the slope of the correlation is significantly shallower than that observed for the Fraser River basin at the 95% confidence level. Interestingly, the Nelson River basin that drains the North American interior to the Hudson Bay, extends this linear correlation to older mean bedrock ages (766 Myr) and more radiogenic $^{87}Sr/^{86}Sr$ of 0.71463 (blue symbols and line in Figure 4a and Table 2).

[18] Published data on the $^{143}Nd/^{144}Nd$ of suspended particles in tributary basins of the Mississippi River basin and other large river basins (Chao Phraya, Chang Jiang, Hong, Hudson, Mackenzie, Mekong, Xi Jiang) define a linear correlation with a slope that is significantly shallower, and a zero-age intercept that is significantly less radiogenic, than that defined by data from the Fraser River system (blue symbols and line in Figure 4b and Table 2). However, anthropogenic modifications in many drainage basins, particularly the trapping of sediment behind dams and enhanced erosion caused by changes in land use [*Wilkinson and McElroy*, 2007], complicates the use of $^{143}Nd/^{144}Nd$ data of suspended matter in rivers for understanding erosive processes in anthropogenically modified drainage basins.

Table 4 (Sample). Summary Data for the 19 Large-Scale Drainage Regions[a] [The full Table 4 is available in the HTML version of this article]

ID	Drainage Region	A_T (km^2)	T_e (Myr)	Seds. (%)	Extr. (%)	Endog. (%)	A_b (km^2)	N	A%	Q_b SS (Mt yr^{-1})	N	Q SS %	Q_{AT} SS (Mt yr^{-1})	Q_b (km^3 yr^{-1})	N	Q%	Q_{AT} (km^3 yr^{-1})	c Sr_d (μg l^{-1})	$^{87}Sr/^{86}Sr_w$
1	Russian Arctic	13,087,208	364	80.3	6.9	12.8	11,444,776	40	87.5	100	22	84.8	118	2,472	37	87.3	2,833	90	0.7102
2	N. American Arctic	3,577,966	706	79.9	3.7	16.5	2,830,837	18	79.1	335	10	70.1	478	663	15	76.6	866	165	0.7111
3	E. North America	9,325,220	499	73.0	8.2	18.8	7,675,141	117	82.3	491	38	65.2	753	2,266	107	81.4	2,784	118	0.7105
4	W. Europe	1,998,839	310	65.0	6.1	28.9	1,585,093	246	79.3	32	34	49.1	65	632	234	74.6	848	408	0.7093
5	E. South America	16,369,568	390	66.3	9.5	24.2	14,083,213	100	86.0	1,841	55	77.4	2,378	9,597	90	85.7	11,197	28	0.7125
6	W. Africa	11,261,691	634	63.9	1.8	34.4	9,712,254	69	86.2	256	24	72.7	352	2,077	49	82.8	2,510	22	0.7150
7	E. Africa	5,701,908	637	56.8	9.6	33.6	4,824,018	61	84.6	167	13	39.9	419	359	54	79.4	452	148	0.7120*
8	Arabia-India-SE Asia	9,590,213	346	69.2	9.5	21.3	6,005,778	69	62.6	2,424	31	56.3	4,304	2,693	58	60.9	4,419	165	0.7144
9	East Asia	14,073,715	231	72.3	14.2	13.4	9,544,451	210	67.8	2,689	92	58.2	4,622	4,616	172	64.8	7,127	185	0.7104
10	W. North America	5,405,659	173	47.4	35.0	17.6	3,806,397	94	70.4	562	57	58.3	965	1,197	81	69.8	1,715	127	0.7108
11	W. South America	1,220,853	96	38.0	37.3	24.7	661,283	86	54.2	55	6	4.7	1,171	597	72	47.2	1,266	43	0.7057
12	Australia-NZ	4,701,839	580	79.5	5.1	15.4	3,743,781	207	79.6	214	92	40.4	530	369	125	65.1	566	127	0.7123
13	Antarctica (≥60°S)	1,523,722		29.0	22.7	48.4													
14	Mediterranean	5,726,983	253	77.9	4.6	17.6	4,108,421	123	71.7	442	80	64.7	683	389	100	69.3	561	354	0.7077
15	Caspian Sea	8,049,943		93.3	1.9	4.8	4,157,743	10	51.6	192	6	39.3	490	524	9	51.6	1,016		0.7082
16	Black Sea	2,453,129	187	84.4	4.6	11.0	2,175,984	25	88.7	184	19	88.2	209	365	19	88.2	414	235	0.7088
17	Red Sea	935,189		23.4	30.9	45.7													
18	Baltic Sea	1,846,881	672	58.5	0.0	41.5	1,553,992	56	84.1	5	24	65.0	7	426	62	79.8	534	116	0.7120
19	Hudson Bay	3,753,826	1,549	46.7	8.1	45.3	2,792,775	24	74.4	2	4	6.5	26	619	24	74.4	833	29	0.7172
Sum		120,604,352		69.7	8.8	21.5	90,705,936	1,555	75.2	9,991	607	60.5	17,570	29,862	1,308	73.0	39,941		
Sum exoreic		110,095,498					86,548,194	1,545	78.6	9,799	601	63.4	17,081	29,338	1,299	76.2	38,925	110	0.7111*
T_{ew} (Myr)		445					453			342			328	405			394		
εNd		−10.1					−10.3			−7.8			−7.4	−9.2			−9.0		
%Seds		68.8					69.0			69.3			67.2	67.9			67.5		
%Extr.		9.4					9.0			11.5			13.3	10.4			11.0		
%Endog.		21.8					22.0			19.2			19.5	21.7			21.4		

[a]Abbreviations are as follows: ID, number of large-scale drainage region [*Graham et al.*, 1999, 2000]; A_T, total exorheic land area in km^2; T_e, average bedrock age, in Myr, calculated with an exponential age model; Seds., Sedimentary bedrock; Extr., extrusive bedrock; Endog., endogenous bedrock; A_b, best estimate of exorheic land area, in km^2, for which the database has entries; N, number of river basins; A %, percent of total exorheic land area for which the database contains data; Q_b SS, best flux estimate (Mt yr^{-1}) of suspended sediment for which the database contains data; Q SS%, percent of total exorheic suspended sediment flux for which the database contains data; Q_{AT} SS, same as above, but extrapolated to entire exorheic land area; Q_b, best estimate of annual water flux (km^3 yr^{-1}) for which the database contains data; Q%, percent of global annual water flux for which the database contains data; Q_{AT}, same as above but extrapolated to entire exorheic land area; c Sr_d, weighted (by water flux and concentration) average dissolved Sr concentration (μg l^{-1}); $^{87}Sr/^{86}Sr_w$, weighted (by water flux and Sr concentration) $^{87}Sr/^{86}Sr$. Asterisk indicates estimated value for East Africa assuming the value for this drainage area plots on the global correlation line. If the uncorrected $^{87}Sr/^{86}Sr$ value of 0.7220 had been used for East Africa the global average $^{87}Sr/^{86}Sr$ would have been 0.7113 instead of 0.7111. A_b Sr, best estimate of exorheic land area (km^2) for which the database contains Sr isotope data; %total, percentage of the total area, water flux or suspended sediment load (respective column to the immediate left); Q_b Sr, best estimate of the annual water flux (km^3 yr^{-1}) for which the database contains Sr isotope data; Q_{AT} Sr, best estimate of the annual water flux (km^3 yr^{-1}) for which data database contains Sr isotope data, adjusted to the entire exorheic water flux; Q_S Sr, specific annual flux of Sr per square kilometer (kg yr^{-1} km^{-2}); Q_P Nd, annual flux (tons yr^{-1}) of particulate Nd; ε_{Nd} $(0)_{Pw}$, weighted (by suspended sediment load) $^{143}Nd/^{144}Nd$ of the suspended matter, expressed in epsilon units; A_b Nd, best estimate of exorheic land area (km) for which the database has Nd isotope data; Q_b Nd, best estimate of the flux of suspended particulate matter (Mt yr^{-1}) for which the database contains Nd isotope data; Q_{AT} Nd, best estimate of the annual flux of suspended particulate matter (Mt yr^{-1}), adjusted to the entire exorheic suspended sediment flux. The rows labeled T_{ew} (Myr) and ε_{Nd} denote the weighted bedrock ages and ε_{Nd} values of various parameters listed in the first row. The parameter ε_{Nd} has been calculated by using average weighted bedrock age (row above) and the linear correlation of large-scale drainage basins shown in Figure 4b (Table 2). The last three rows show relative area percentages of sedimentary (%Seds.), extrusive (%Extr.), and endogenous (%Endog.) bedrock in exorheic drainage area, weighted according to the respective parameter listed in the column header.

3.5. Strontium Isotope Systematics and Sr Fluxes in Large-Scale Continental Drainage Regions

[19] In order to investigate regional correlations between bedrock geology and the dissolved $^{87}Sr/^{86}Sr$ of continental runoff we have compiled data on the dissolved $^{87}Sr/^{86}Sr$ and Sr concentration of 193 rivers and grouped them into 19 large-scale drainage regions that cover the nonglaciated land surface (Data Set S1 and Table 4). Average $^{87}Sr/^{86}Sr$ of continental runoff from these regions are then computed by first weighting Sr concentrations, isotope compositions and water discharges of individual rivers, then summing up all contributions from rivers from the respective drainage region and finally extrapolating these fluxes to the ice-free surface area of the entire drainage region, assuming that the river basins we have data for accurately represent runoff from the respective drainage region. The extent to which we extrapolate is depicted in the pie charts shown in Figure 4a. Some of the large-scale drainage regions are well characterized. For instance, 24 rivers representing 78% of the

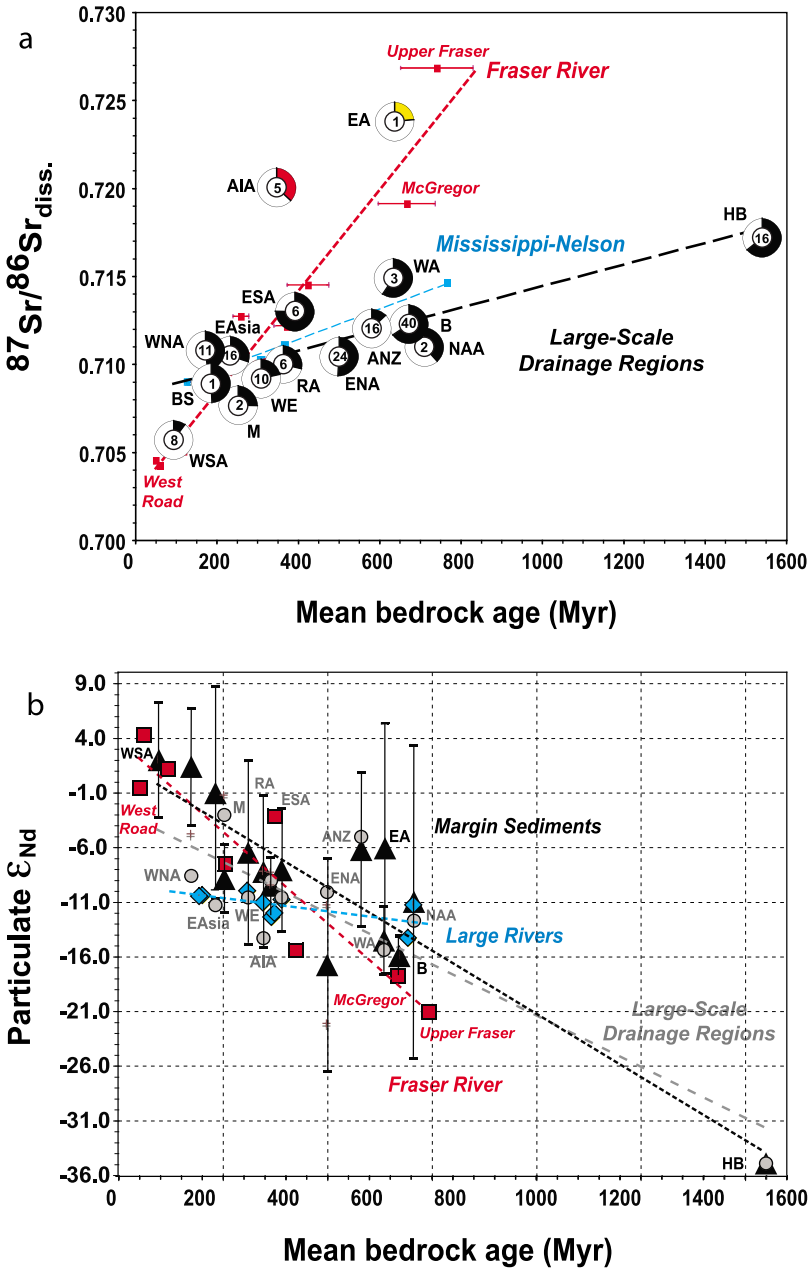

Figure 4

drainage area of, and 51% of the water discharging from eastern North America have been characterized for dissolved $^{87}Sr/^{86}Sr$. In contrast, the dissolved $^{87}Sr/^{86}Sr$ of runoff from western South America has been characterized in only 9 rivers that represent only 17% of this drainage area, and 10% of the total water discharge [*Fiege et al.*, 2009]. In total, data for 193 rivers representing 50.3% of the exorheic land surface and 48.3% of the global exorheic water discharge (38,900 $km^3\ yr^{-1}$) define the flux and isotope composition of continental Sr to the ocean. The correlation between average bedrock ages (in Myr) and dissolved $^{87}Sr/^{86}Sr$ for most of these large-scale drainage regions have a slope and zero-age intercept that are indistinguishable from those of the Mississippi-Nelson trend (Figure 4a and Table 2). Notable exceptions to this correlation are the drainage regions of Arabia, India, and southeast Asia and that of East Africa. The latter is an artifact because the $^{87}Sr/^{86}Sr$ of runoff from this area is determined mainly by data for the Zambezi River that drains large areas of the old and radiogenic East African craton. In contrast, the average bedrock age for this region represents a drainage region that also contains significant areas of younger volcanic and sedimentary bedrock. In contrast to East Africa, data for 8 rivers covering 58% of the drainage region of Arabia, India, and southeast Asia that generates 37% of the water discharge from a region that includes many of the large rivers that drain the Himalaya indicate that this region creates anomalously radiogenic runoff [e.g., *Edmond*, 1992].

[20] The drainage region of western South America that drains the Andean Cordillera into the southeastern Pacific is notable for its unradiogenic $^{87}Sr/^{86}Sr$ and young mean bedrock age of 96 Myr [*Fiege et al.*, 2009]. The position of this region in the $^{87}Sr/^{86}Sr$ bedrock age diagram makes it difficult to discern whether this region is part of the "steep" (Fraser-like) or the "shallow" (Mississippi-Nelson-like) correlation. Making this distinction awaits bedrock data with higher spatial resolution for smaller drainage basins and subbasins, as well as more extended characterization of the dissolved Sr load of rivers that drain this region.

[21] The database enables us to investigate two potentially important factors that could modify the flux of continental Sr to the coastal ocean: water discharge and detrital sediment flux. While data for individual rivers show a significant positive correlation between the specific Sr flux and water flux (cm yr^{-1}), data for large-scale drainage regions do not (Figure 5 and Table 2). Rivers in the drainage region of Australia and New Zealand control most of the positive correlation observed in individual rivers, with Australian rivers having low specific Sr yields and low runoff whereas rivers in New Zealand, particularly those sourced in easily erodable lithologies, are characterized by high specific Sr yields and high runoff. That bedrock geology exerts a major control on this relationship is also seen in the Baltic Sea drainage. Runoff from the low-lying, mostly Precambrian shield areas to the north yield about an order of magnitude less Sr per area than equally intense runoff from the south that is dominated by Phanerozoic sedimentary bedrock that include Sr-rich marine carbonates and evaporates, globally important sources of dissolved riverine Sr with well-constrained isotopic compo-

Figure 4. (a) Relationship between bedrock age and $^{87}Sr/^{86}Sr$ of the dissolved load in the Fraser River basin (red symbols), a variety of large rivers (blue symbols, Hudson, Mackenzie, Mekong, Mississippi, Missouri, Ohio, Song Hong, Xi Jiang, and Chang Jiang), and large-scale drainage regions (black and white pie diagrams). Outliers in the large-scale drainage regions are highlighted in red (Arabia, India, and southeast Asia) and yellow (East Africa). The filled area of each pie diagram shows that fraction of the total water flux that has been characterized for dissolved $^{87}Sr/^{86}Sr$. Abbreviations are as follows: AIA, Arabia, India, and southeast Asia; WNA, western North America; ENA, eastern North America; NAA, North American Arctic; ESA, eastern South America; WSA, western South America; RA, Russian Arctic; WE, western Europe; BS, Black Sea; EAsia, East Asia; EA, East Africa; ANZ, Australia and New Zealand; WA, western Africa; M, Mediterranean; B, Baltic Sea; HB, Hudson Bay. Numbers in the centers of the pie diagrams indicate the number of rivers that have been analyzed for Sr isotope composition. The linear regression lines represent linearized decay equations ($R_0 = R_t + P/D\lambda t$) that are valid if $t \ll \tau$. Subscripts 0 and t refer to today and geologic age of formation, respectively; R is the respective isotope ratio; P/D is the ratio of the parent isotope to the isotope of daughter element used for normalization (e.g., $^{87}Rb/^{86}Sr$); and λ and τ are the decay constants and half-lives, respectively. (b) Relationship between bedrock age and $^{143}Nd/^{144}Nd$ of the particulate load in the Fraser River basin (red squares and line); the Mississippi, Hudson, Mackenzie, Mekong, Song Hong (Red), Xi Jiang (Pearl), and Chang Jiang (Yangtze) river basins (blue diamonds and line); and large-scale drainage regions (gray circles and line), as well as clastic marine sediments deposited along the continental margins (black triangles with 1 standard deviation uncertainties and line, based on raw data from *Jeandel et al.* [2007] and *Arsouze* [2008]). Abbreviations as in Figure 4a.

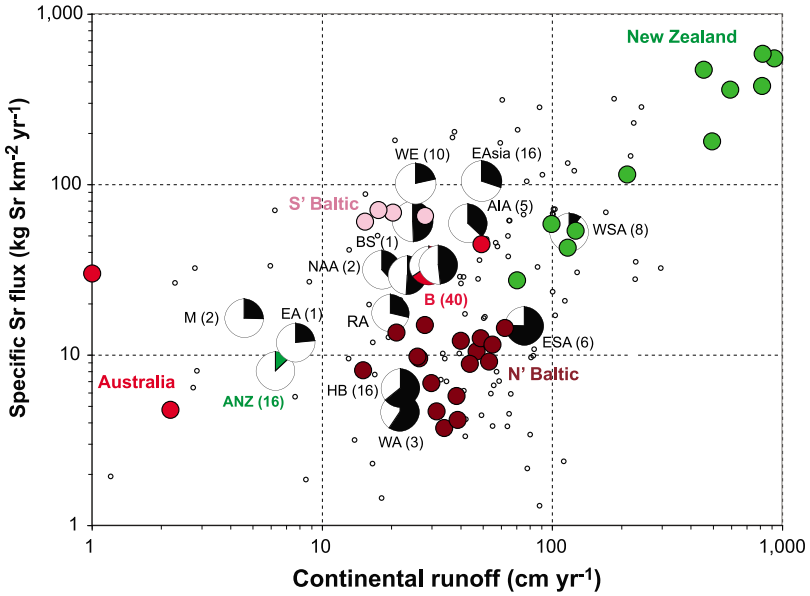

Figure 5. Specific flux of strontium (kg Sr km^{-2} yr^{-1}) versus continental runoff (i.e., specific annual water flux in cm yr^{-1}). Individual river basins are shown as small circles, and large-scale drainage regions are depicted as black and white pie circles, with the filled pie area representing the fraction of the total water flux that has been characterized for dissolved $^{87}Sr/^{86}Sr$ and Sr concentration. Individual river basins discussed in the text are highlighted: red circles, rivers in Australia; green circles, rivers in New Zealand; pink circles, rivers draining the southern portion of the Baltic Sea drainage; brown circles, rivers draining the Fennoscandian Shield to the north of the Baltic Sea. Abbreviations are identical to those used in Figure 4.

sition. Anthropogenic alteration (e.g., mining of evaporite deposits, land use changes) of southern drainage basins likely contributes to high specific Sr yields in rivers entering the Baltic Sea from the south. While data for individual rivers could be used to argue that doubling of runoff causes a ~50% increase in specific Sr yield, data for large-scale drainage regions do not support such a correlation.

[22] The correlation between specific Sr flux and suspended sediment yield has a shallow, but significant positive slope of 0.028 ± 0.008 (see Table 2) that requires a thirtyfold to fortyfold increase in suspended sediment yield for a twofold increase in the specific dissolved Sr flux (Figure 6). Much of this positive correlation is controlled by the very high specific Sr fluxes in drainage basins with exceptionally high suspended sediment yields in New Zealand, such as the Haast and the Hokitika River basins. The large river basins that drain the Himalaya (Indus, Ganges, Brahmaputra) are characterized by relatively high yields of suspended sediment, but average specific Sr fluxes. Such a positive correlation does not exist if only data for large-scale drainage regions are considered (see Table 2).

[23] Taken together, data on the relationship between specific Sr flux on one hand and water flux and specific suspended sediment yield on the other hand indicate that the capacity for high dissolved Sr yields is primarily controlled by bedrock geology (e.g., Sr-rich carbonates and evaporites) rather than water or suspended sediment fluxes. Further investigations are needed to evaluate the importance of other factors, such as topographic gradient, vegetation, soil type and thickness, and anthropogenic modifications of river basins [e.g., *Hicks et al.*, 2004].

[24] We emphasize that the globally weighted Sr concentration based on our data compilation is 111 $\mu g\ l^{-1}$ (1.27 μM). This estimate was computed using Sr concentrations and water fluxes of individual rivers that were then extrapolated to the surface area of the nonglaciated exorheic drainage regions. The estimate is significantly higher than the Sr concentration that is calculated by weighting all rivers analyzed for Sr isotopic composition according to Sr concentration and water flux alone, without regional averaging (80 $\mu g\ l^{-1}$ or 0.91 μM). The latter estimate is very similar to most previous estimates that appear to underestimate the riverine Sr flux to the ocean, and thus overestimate the marine residence time of Sr (see compilation by *Vance et al.* [2009]). The latter statement is true only if the database and method of regional averaging

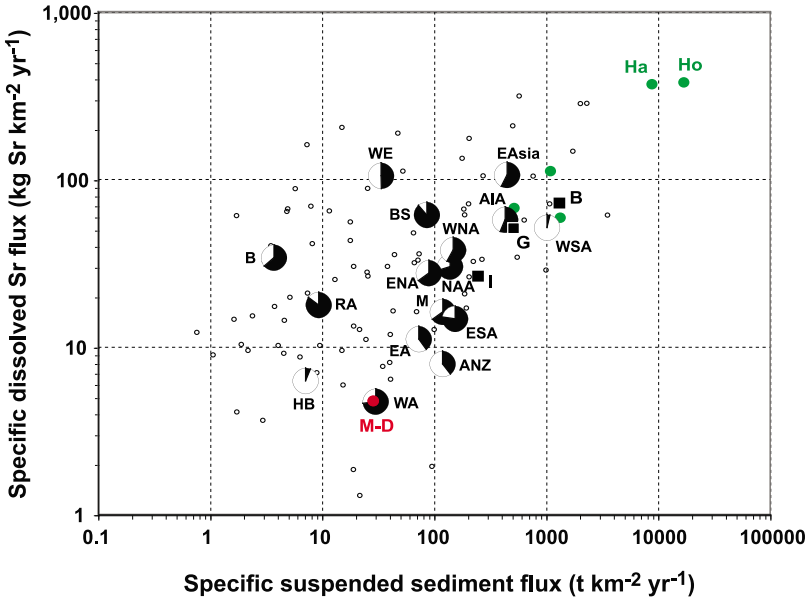

Figure 6. Specific flux of dissolved Sr (kg Sr km^{-2} yr^{-1}) versus specific suspended sediment yield (tons km^{-2} yr^{-1}). Individual river basins are shown as small circles, and large-scale drainage regions are depicted as pie circles, with the filled pie area representing the fraction of the total suspended sediment load from each region we have data on the suspended sediment load for. Individual river basins discussed in the text are highlighted with the same color code as in Figure 5 (M-D, Murray-Darling (Australia); Ha, Haast; Ho, Hokitika (both in New Zealand)). In addition, rivers draining the Himalaya are shown as large black squares (I, Indus; G, Ganges; B, Brahmaputra (all in region AIA, Arabia, India, and southeast Asia)). Abbreviations are identical to those used in Figures 4 and 5.

does not introduce systematic bias. One potential bias might derive from the use of data on concentration and $^{87}Sr/^{86}Sr$ that were made overwhelmingly after the 1970s, and thus after significant modifications of most river basins had occurred. Yet water, and thus Sr, fluxes are calculated using predam or natural discharge estimates [*Peucker-Ehrenbrink*, 2009]. If we use available postdam water discharge data, the average Sr concentrations of runoff from drainage regions 9 (East Asia) and 10 (western North America) are reduced from 205 to 192 μg Sr l^{-1} and 124 and 101 μg Sr l^{-1}, respectively, and the global average decreases from 111 to 108 μg Sr l^{-1}. The $^{87}Sr/^{86}Sr$ is not significantly affected by these changes. Also noticeable in the database are high Sr concentrations in regions where water use for human needs (agriculture, mining, land use change) is intense, such as some of the large river basins in western Europe (e.g., Rhone, Rhine, Elbe), North Africa (Nile), North America (Mississippi) and Australia (e.g., Murray-Darling). These anthropogenic effects may also bias the average global Sr concentration in rivers toward higher values [*Palmer and Edmond*, 1989]. Finally, it is worthwhile to point out that we lack sufficient data on smaller coastal watersheds that are underrepresented in all global databases, including the most comprehensive Land2Sea database [*Peucker-Ehrenbrink*, 2009]. If these coastal rivers have different Sr concentration or $^{87}Sr/^{86}Sr$ (i.e., younger bedrock ages) than the remainder of the drainage regions for which data exist, simple extrapolation to include those uncharacterized areas may introduce additional bias. In light of these uncertainties it is possible that the older average global Sr concentrations more closely resemble preanthropogenic values, albeit for the wrong reasons. It is clear that the lower estimates are caused by the overrepresentation of large rivers with low Sr concentrations (e.g., Amazon, Congo) because fluxes for well-characterized rivers are simply extrapolated to the global runoff, and thus weighted more heavily. The Amazon that delivers 15%–18% of the global water flux to the ocean usually accounts for more than one quarter of the water flux that has been characterized in previous studies. Unless water discharges are regionally averaged, as in this study, global averages that are based on extrapolation from well-studied rivers without regional averaging will be biased toward lower Sr concentrations. We consider it likely that the underrepresentation of small coastal rivers leads to an overestimation of the $^{87}Sr/^{86}Sr$ of continental runoff, because most coastal areas are dominated by younger sedimentary (passive margins) and volcanic (active margins) bedrock that tend to generate less radiogenic runoff. In section 3.6 we

attempt to quantify uncertainties in the Sr concentration and $^{87}Sr/^{86}Sr$ using the Amazon River system as an example.

3.6. Uncertainties of Riverine Fluxes and Isotope Compositions

[25] Often cited values for the Amazon River are 0.32 μM Sr and $^{87}Sr/^{86}Sr$ of 0.7109 [*Palmer and Edmond*, 1989], 0.317 μM Sr and $^{87}Sr/^{86}Sr$ of 0.7109, and 0.346 μM Sr and $^{87}Sr/^{86}Sr$ of 0.7108 [*Palmer and Edmond*, 1992]. These samples were collected at Obidos, upstream of the confluences with the Tapajos and Xingu rivers. *Palmer and Edmond* [1989] report values of 0.10 μM Sr and $^{87}Sr/^{86}Sr$ of 0.7322 for the Tapajos and 0.156 μM Sr and $^{87}Sr/^{86}Sr$ of 0.7292 for the Xingu. *Vance et al.* [2009] correct for the omission of the Tapajos and Xingu rivers in the Amazon mass balance by including all three rivers in their data compilation. However, they use the total flow of the Amazon (6590 km^3 yr^{-1}) plus that of the Tapajos (489 km^3 yr^{-1}) and the Xingu (505 km^3 yr^{-1}) rivers, yielding a total Amazon water discharge of 7584 km^3 yr^{-1}, a value that is larger than most cited discharge values. The often cited annual water discharge values for the Tapajos (489 km^3 yr^{-1}) and Xingu (505 km^3 yr^{-1}) rivers are erroneous, as those values represent ~1/1000 of the drainage basin area, suggestive of a conversion error in previous publications. The SAGE database lists long-term average discharge values for these rivers at 340 ± 33 km^3 yr^{-1} (1973–1994) and 268 ± 50 km^3 yr^{-1} (1971–1997). The long-term average discharge of the Amazon at Obidos is listed at 5417 ± 618 km^3 yr^{-1}. If these values are used in conjunction with the above data on Sr concentration and $^{87}Sr/^{86}Sr$, the average Sr concentration of the combined Amazon, Tapajos and Xingu rivers is 0.31 μM with an average $^{87}Sr/^{86}Sr$ of 0.71165. We take these values as representative of the total water discharge of the Amazon River system (6300 km^3 yr^{-1}), a value that is uncertain by at least 10%. We also note that dissolved Sr concentrations of the Amazon decrease slightly with increasing water discharge [*Seyler et al.*, 2003]. *Palmer and Edmond* [1992] sampled the Amazon at Obidos in June 1976 and 1977 under high-flow conditions. The Sr concentrations of 0.317 and 0.346 μM are therefore likely minimum values. In contrast, the Sr concentrations of the Tapajos (0.100 μM) and Xingu (0.156 μM) rivers represent low- to medium-low-flow conditions in June 1976, a year of rather low discharge. It is thus likely that both Sr concentrations are above average. The above isotope mass balance may therefore overestimate the isotope contributions from the Tapajos and Xingu rivers and underestimate the contribution from the Amazon at Obidos, making the bulk Sr flux too radiogenic. How the isotope composition changes with water discharge is not known. The total annual Sr flux calculated here (0.171 Mt yr^{-1}) is slightly higher than that calculated by *Vance et al.* [2009] for the combined Amazon, Tapajos and Xingu (0.159 Mt yr^{-1}), but both are lower than the flux calculated using the monthly time series data of Sr and runoff (0.205 Mt yr^{-1} [*Seyler et al.*, 2003]), indicating that Sr fluxes based on few data are uncertain by at least 20%, even for a hydrologically less dynamic river such as the Amazon. Reducing uncertainties in river fluxes and isotope composition require long-term time series data of Sr concentration and isotope composition. Even if we had such data it remained uncertain how accurately well-established present-day estimates represented preanthropogenic conditions [e.g., *Palmer and Edmond*, 1989, 1992].

3.7. Neodymium Isotope Systematics of Large-Scale Continental Drainage Regions

[26] We also use the Land2Sea database [*Peucker-Ehrenbrink*, 2009] in conjunction with Nd concentrations (62 rivers) and isotope compositions (79 rivers) in 19 large-scale drainage regions [*Graham et al.*, 1999, 2000] to compute the weighted Nd isotope composition of detrital matter delivered to the ocean margins. Neodymium isotope values are first weighted according to Nd concentration and annual suspended sediment fluxes of each river within a drainage region. We use an average upper crustal Nd concentration of 26 μg g^{-1} [*McLennan*, 2001] whenever no data on Nd concentration in particulate matter is available. Then, the Nd flux from all the river basins we have data for within each large-scale drainage region is extrapolated to the total surface area of the respective large-scale drainage region to yield the Nd flux from each large-scale drainage region. The database enables us to evaluate whether the estimated average Nd isotope composition could be biased with respect to bedrock lithology and age, two important parameters that influence the Nd isotope composition and concentration of continental inputs to the ocean. We assume that the weighted isotope composition of riverine suspended matter is equal to the isotope composition of material delivered to the ocean basins. This assumption is valid if differences in the degree to which estuaries modify Nd fluxes and isotope compositions are small between the various large-scale drainage regions. We do not yet have sufficient

data to evaluate how significantly anthropogenic modifications of drainage basins (e.g., damming, land use changes) have altered the flux and isotope composition of detrital sediment transported to the coastal ocean. However, we do recognize that the present-day flux and isotope composition of riverine particulate matter may no longer reflect the natural delivery process of particulate matter by rivers [*Syvitski et al.*, 2005; *Wilkinson and McElroy*, 2007; *Chao et al.*, 2008; *Syvitski and Kettner*, 2008]. In section 3.8 we therefore use the isotope composition of clastic sediments deposited along ocean margins as a proxy for the preanthropogenic isotope composition of land-derived material. Such sediments are much less affected by recent anthropogenic changes, specifically damming, than modern river suspended particles, and may therefore yield additional insights into the nature of correlations between bedrock age and isotope composition.

3.8. Neodymium Isotope Systematics of Detrital Sediments Deposited Along Ocean Margins

[27] Detrital sediments along continental margins provide another perspective of the delivery of continental detritus to the ocean. This perspective is limited to Nd because of its high concentration in detrital minerals and low concentrations in marine carbonates that dilute continental margin sediments to various degrees, as is the case for Sr. We compare the data for rivers discussed above with data on margin sediments compiled by *Jeandel et al.* [2007] and *Arsouze* [2008]. This data is first grouped into the 19 large-scale drainage regions, and then regionally averaged without taking the small variations in Nd concentration between samples into account. With the exception of the east coast of North America we made no attempt to correct for regional sampling biases within individual drainage regions. The data for the east coast of North America, however, are strongly biased toward samples from high latitudes that receive preferential input from the unradiogenic Canadian Shield. In order to correct for this bias we weighted equally all margin sediments north of 55°N ($\varepsilon_{Nd} = -24.3$) on one hand and the suspended particulates of the Hudson ($\varepsilon_{Nd} = -11.3$), Mississippi ($\varepsilon_{Nd} = -10.9$) and St. Lawrence ($\varepsilon_{Nd} = -5.3$) rivers as proxies for continental detritus south of 55°N on the other hand. This correction raises the average ε_{Nd} of this large drainage region from $\varepsilon_{Nd} = -22$ to $\varepsilon_{Nd} = -16.7$. If the detrital load of the Mississippi ($\varepsilon_{Nd} = -10.9$) were weighted even more strongly the above estimate shifted even closer toward the linear regression line. The uncertainties shown in Figure 4b are the standard deviations of the averages of all data from the respective drainage region. The slope and intercept of the linear regression of margin sediments (black symbols and line in Figure 4b and Table 2) are statistically indistinguishable (95% CI) from the slope and intercept of the regression of the data for individual rivers (gray symbols and line in Figure 4b and Table 2), thus confirming the conclusion of *Jeandel et al.* [2007] and *Arsouze* [2008] that the geology of adjacent continental margins can be used as a proxy for the isotope composition of continental inputs to the ocean.

4. Discussion

4.1. Sr and Nd Isotope Systematics of Individual River Drainage Basins

[28] The $^{87}Sr/^{86}Sr$ age trends can be interpreted either as radiogenic ingrowth trajectories with average effective $^{87}Rb/^{86}Sr$ of ~2 (Fraser basin) and ~0.6 (Mississippi basin), or as two-component mixing of young unradiogenic with old radiogenic end-members. The main difference between both basins is the much more radiogenic $^{87}Sr/^{86}Sr$ mobilized from the old end-member in the Fraser basin. This end-member is dominated by Precambrian metamorphic and Paleozoic-Precambrian sedimentary rocks. We argue that two factors contribute to this difference. First, Sr is lost preferentially to Rb during incongruent weathering, causing elevated $^{87}Rb/^{86}Sr$ and ingrowth of radiogenic $^{87}Sr/^{86}Sr$ in weathering products [*Dasch*, 1969; *Goldstein and Jacobsen*, 1987, 1988; *Goldstein*, 1988; *Cameron and Hattori*, 1997; *Gaillardet et al.*, 1999]. Consequently, the $^{87}Rb/^{86}Sr$ of the Fraser River particulate load correlates positively with the abundance of predominantly old sedimentary rocks in tributary basins (Figure 7). The $^{87}Rb/^{86}Sr$ of particulate matter of 2–4 in the upper Fraser River is significantly larger than the average $^{87}Rb/^{86}Sr$ of continental crust (0.4 [*McLennan*, 2001]), global subducting sediments (GLOSS: 0.5 [*Plank and Langmuir*, 1998]), or the average Canadian Shield (1 [*Shaw et al.*, 1986]). This is consistent with our contention that differences in dissolved $^{87}Sr/^{86}Sr$ are partly caused by differences in $^{87}Rb/^{86}Sr$ of the old bedrock end-members. The greater susceptibility of the Sr isotope system to secondary overprint (e.g., loss of dissolved Sr, retention of Rb by clays) compared with the Nd isotope system causes Sr model ages of suspended matter to be younger than Nd model ages, both of which are older than present-day bedrock ages

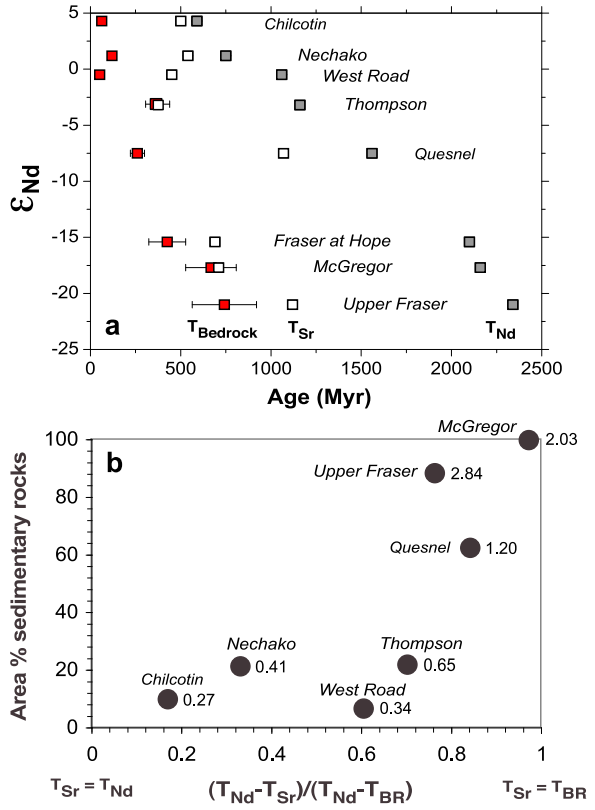

Figure 7. (a) Relationship between the Nd isotope composition of suspended particulate matter (ε_{Nd}) and their respective Nd (gray squares) and Sr (white squares) model ages, as well as the mean bedrock age (red squares) of the respective tributary basins of the Fraser River basin. Uncertainties are 1 standard deviation and are smaller than the symbols whenever the error bars are not visible. (b) Relationship between the extent by which the Rb/Sr system of suspended particulate matter has been disturbed and the abundance (in %) of sedimentary bedrock in tributary basins of the Fraser River basin. The extent of disturbance of the Rb/Sr isotope system is expressed with the parameter $(T_{Nd} - T_{Sr})/(T_{Nd} - T_{BR})$, with T_{Nd} = Nd model age [*Cameron and Hattori*, 1997], T_{Sr} = Sr model age [*Cameron and Hattori*, 1997], and T_{BR} = mean bedrock age (this study). A numerical value of 0 means no secondary overprint, as Nd and Sr model ages are identical. A numerical value of 1 means that the Sr model age is identical to the mean bedrock age, indicating complete resetting of the Sr model ages. Neodymium model ages are considered essentially unaffected by erosion, weathering, and cannibalistic recycling of sedimentary rocks. Numbers to the right of the black circles refer to $^{87}Rb/^{86}Sr$ values of the suspended particulate matter in each tributary drainage basin. High values indicate preferential retention of Rb on clay minerals and loss of Sr during weathering. All data except mean bedrock ages are from *Cameron and Hattori* [1997].

(Figure 7b). The extent to which Sr model ages are reset toward bedrock ages (i.e., depositional ages of sediments) and thus differ from Nd model ages is largely controlled by the abundance of sedimentary rocks in the respective drainage basins (Figure 7b).

[29] Second, incongruent weathering can preferentially mobilize Sr with an isotopic composition different than the bulk rock [*Dasch*, 1969; *Blum and Erel*, 1995] and thus contribute to the observed contrast in $^{87}Sr/^{86}Sr$. Incongruent weathering processes strongly affect river chemistry under weathering-limited conditions where rapid physical erosion limits the formation of deep soils [*Stallard and Edmond*, 1983]. In transport-limited weathering regimes, weathering reactions proceed toward a new equilibrium and bedrock is overlain by deeply weathered soils. Based on the above characteristics, the Fraser and the Mississippi River basins can be viewed as examples of more strongly weathering-limited versus transport-limited environments, respectively. The different slopes in Figure 4a could thus be viewed as reflecting an immature, weathering-limited drainage basin, the Fraser, with old weathering products in the mountainous headwater basins, versus a mature, transport-limited drainage basin, the Mississippi, with only small areas of recently exposed, low-relief Precambrian basement in its headwater basins. The Nelson River basin (average bedrock age of 766 ± 23 Myr), a predominantly transport-limited basin that borders the Mississippi River basin to the north, extends the trend defined by the Mississippi River to older ages, thus confirming our interpretation.

[30] $^{87}Sr/^{86}Sr$ "hot spots," i.e., areas of relatively young bedrock that generate unusually radiogenic runoff, cannot only dominate individual river basins, but also large-scale drainage regions. The large-scale drainage region of Arabia, India, and southeast Asia is the only region that diverges from the global trend toward much more radiogenic runoff. Metasedimentary rocks, particularly in the Lesser Himalaya, are known for their unusually radiogenic $^{87}Sr/^{86}Sr$ that may result from metamorphic redistribution of radiogenic Sr from old, radiogenic precursors [e.g., *Edmond*, 1992; *Galy et al.*, 1999]. The presence of such rocks and the fact that these areas are affected by exceptional uplift and erosion rates may explain why the $^{87}Sr/^{86}Sr$ of runoff from this large region is significantly more radiogenic than would be expected based on the average bedrock age of the region. The fact that we did not weight bedrock ages according to precipitation, water discharge, topographic gradient, Sr concentration,

Table 5. Comparison of Some Literature Estimates of Average Sr Concentration, Flux, and $^{87}Sr/^{86}Sr$

Reference	Water Flux Characterized ($km^3\ yr^{-1}$)	Average Sr Concentration ($\mu mol\ kg^{-1}$)	Global Sr Flux (10^{10} mol)	Average $^{87}Sr/^{86}Sr$
Goldstein and Jacobsen [1987]	9,868	0.705		0.7101 (5)
Palmer and Edmond [1989][a]	18,721.8	0.890	3.33	0.7119
Palmer and Edmond [1989][b]	21,708.8	0.923	3.54	0.7114[c]
Vance et al. [2009]	23,966[d]		3.37	0.71144
This study	19,566	1.22[e]	4.7	0.7111[f]

[a]Based on river data.
[b]Includes estimates for regions based on bedrock geology.
[c]Assuming $^{87}Sr/^{86}Sr = 0.7111$ for uncharacterized areas and $^{87}Sr/^{86}Sr = 0.7117$ for all measured and estimated rivers.
[d]Includes runoff from areas that have been characterized by a fraction of the total runoff, e.g., Baltic Sea, Indonesia, Philippines, and Japan.
[e]Includes only using postdam water discharge data for East Asia and western North America.
[f]Using an estimate of $^{87}Sr/^{86}Sr = 0.7120$ for runoff from East Africa.

or weatherability may also introduce unspecified bias.

4.2. Global Continental Input of Dissolved Sr to Seawater

[31] Based on our data compilation and analysis the average dissolved Sr concentration of global river water is 1.22 μmol Sr kg^{-1} ($^{87}Sr/^{86}Sr = 0.7113$), equivalent to a total annual flux of 4.8×10^{10} mol Sr, significantly higher than previous estimates (Table 5). Our estimate has not been corrected for anthropogenic effects. We hypothesize that previous lower flux estimates result primarily from extrapolating data from a few larger rivers with lower Sr concentration (e.g., Amazon, Congo, Orinoco) to global runoff. This "Amazon effect" can be mitigated if relevant parameters are first regionally averaged and then extrapolated to the globe. If the isotope composition of runoff from East Africa (0.7210, n = 3), that is heavily biased by the radiogenic Zambesi River, is assumed to reflect its bedrock age according to the age-area correlation ($^{87}Sr/^{86}Sr = 0.7120$), the $^{87}Sr/^{86}Sr$ of dissolved riverine Sr delivered to the ocean is 0.7111, a value we consider the best available estimate. The significant spread in $^{87}Sr/^{86}Sr$ of continental runoff from large, reasonably well studied drainage regions, from 0.7057 (western South America) to 0.7172 (Hudson Bay), merits reevaluating the role that temporal changes in bedrock geology, spatial distribution of water discharge, paleogeography and other factors that influence weathering and erosion have had on the temporal evolution of the seawater $^{87}Sr/^{86}Sr$ [e.g., *Brass*, 1976].

[32] The particulate flux of Sr to the coastal ocean (7.4×10^{10} mol Sr), estimated by multiplying the annual suspended sediment flux (1.85×10^{16} g) with the average Sr concentration of the upper continental crust of 350 $\mu g\ g^{-1}$ [*McLennan*, 2001], is less than twice the annual dissolved load. In contrast to Nd, it is unlikely that dissolution of suspended particulate matter in seawater, or addition of Sr during diagenesis of marine sediments of continental origin adds significant continental Sr to seawater. *Elderfield and Gieskes* [1982] found little evidence for significant addition of continental Sr from diffusive diagenetic fluxes. However, the global flux and isotope composition of continental Sr delivered to the ocean by submarine groundwater discharge remains to be quantified [*Basu et al.*, 2001]. Taken together, the greater Sr flux to seawater estimated in this study together with the less radiogenic composition does not significantly modify the apparent imbalance between present-day Sr sources to seawater and the observed secular increase in the $^{87}Sr/^{86}Sr$ of seawater over the Quaternary [e.g., *Palmer and Edmond*, 1989; *Davis et al.*, 2003; *Vance et al.*, 2009]. However, it is important to point out that two potentially important sources of Sr to seawater remain poorly quantified: the advective flux from marine sediments and submarine groundwater discharge. In addition, the present-day Sr flux may not represent pre-anthropogenic conditions and the lack of data for smaller coastal rivers that drain predominantly younger volcanic and sedimentary bedrock may bias current estimates of global riverine $^{87}Sr/^{86}Sr$ to more radiogenic values.

4.3. Sr and Nd Isotope Systematics of Large-Scale Drainage Regions

[33] The observed correlations between isotope composition and age can be interpreted as mixing lines between young and old bedrock lithologies. The fact that present-day isotope composition reflects time-integrated parent-daughter ratios, and thus lithology, mandates the existence of global

correlations between bedrock age, isotope composition and lithology. A global bedrock analysis bears this out [*Peucker-Ehrenbrink and Miller*, 2007]: Volcanic bedrock is mostly young (mean bedrock age of 335 ± 52 million years [Myr], 1 standard deviation) with radiogenic ε_{Nd} and unradiogenic $^{87}Sr/^{86}Sr$. Though on average even younger (246 ± 42 Myr, 1 standard deviation), sedimentary bedrock (including Sr-rich carbonates and evaporates) has slightly less radiogenic ε_{Nd} and more radiogenic $^{87}Sr/^{86}Sr$ dominated by past seawater $^{87}Sr/^{86}Sr$. Endogenous (i.e., plutonic and metamorphic) bedrock, in contrast, is on average much older (1749 ± 269 Myr, 1 standard deviation) with much less radiogenic ε_{Nd} and very radiogenic $^{87}Sr/^{86}Sr$, representing the old end-member of the correlations between isotope composition and age. *Wilkinson et al.* [2009] interpret the difference in bedrock ages between these lithologic units as a result of the locus of the formation of lithologies: sedimentary and volcanic rocks form at or very near the surface and thus have essentially near-zero bedrock ages at the time of formation. Their age-area distributions follow power law relationships, where disappearance of young bedrock with time is achieved foremost through burial by younger units and, to a lesser extent, by exposure and erosion. In contrast, plutonic and metamorphic rocks are formed at depth. The time it takes to bring these lithologies to the surface results in significantly older bedrock ages and age-area distributions that are lognormal.

[34] The relative contributions of continental Sr stemming from drainage areas with steep $^{87}Sr/^{86}Sr$ bedrock age trends as opposed to those stemming from areas characterized by shallower trends can be quantified. If we assume that the $^{87}Sr/^{86}Sr$ of continental runoff estimated above properly characterized global continental inputs of dissolved Sr to seawater, we can use the mean bedrock age of large-scale drainage regions weighted according to their annual water flux (394 Myr) to determine how close the location of this global data points plots in relation to the shallow versus steep correlation lines. This global data point plots close to the Mississippi-Nelson correlation ($^{87}Sr/^{86}Sr$ of 0.7113 instead of 0.7115 at 394 Myr bedrock age) and can be interpreted as a 30/70 mixture of "steep" (i.e., Fraser-like, weathering-limited) versus "shallow" (i.e., Mississippi-like, transport-limited) contributions. The balance between these two sources may have been different in the geologic past, and temporal shifts from "steep" to "shallow" and vise versa may have influenced the isotope composition of seawater. A better understanding of the parameters and processes that control the slope of the $^{87}Sr/^{86}Sr$ bedrock age correlations is needed to link temporal changes in the $^{87}Sr/^{86}Sr$ of seawater to the controlling parameters and processes.

4.4. Boundary Exchange and the Nd Isotope Composition of Seawater

[35] If, as *Tachikawa et al.* [2003], *Lacan and Jeandel* [2005a, 2005b], *Arsouze* [2008], and *Arsouze et al.* [2009] hypothesize, the Nd isotope composition of seawater is primarily determined by complex exchange processes between marine water masses and continental detritus, the correlation between ε_{Nd} and bedrock age of source areas of marine detrital matter could be used to estimate the globally average ε_{Nd} of seawater. The correlation of all margin sediments and particulate matter from large-scale drainage regions has a zero-bedrock age ε_{Nd} of −0.2 and a slope of −0.021 (Table 2). If we weight the average bedrock ages of the large-scale drainage regions according to the mass of suspended particulate matter transported by rivers in each drainage region [*Peucker-Ehrenbrink*, 2009], the average bedrock age of detrital source areas on the continents is ~336 Myr. This age together with the above correlation yield an estimated ε_{Nd} of detrital matter delivered to the global ocean of −7.3 ± 2.2 (standard error). This value is indistinguishable from an independent assessment of the globally averaged ε_{Nd} of seawater of −7.2 ± 0.5 (1 standard deviation) that is based on the geometric mean of the isotope compositions of more than 600 seawater samples from various ocean basins (see section 2 and Table 1). We emphasize that the ε_{Nd} of the Pacific Ocean (−4.1) is biased by the preponderance of data for radiogenic North Pacific seawater. If average Pacific Ocean water were slightly less radiogenic than indicated by the existing seawater data (e.g., ε_{Nd} of −5 instead of −4.1), the global average seawater value shifted from ε_{Nd} of −7.2 to −7.6, presumably with similar uncertainties as determined above. The good correspondence between these independent estimates lends credence to the "boundary exchange" hypothesis. We point out that this reevaluation of continental sources and average seawater brings the average isotope composition of continental detrital input and average seawater in even closer agreement than the earlier assessment by *Goldstein and Jacobsen* [1987] (ε_{Nd} of −8.4 ± 1.0 and −6.5 ± 1.1, respectively), thereby eliminating the need for a radiogenic source, i.e., submarine hydrothermal fluids, to balance the seawater Nd isotope budget.

4.5. Implications for the Evolving Chemical Composition of the Continental Crust

[36] The observed correlations between bedrock ages and radiogenic isotope composition can be used to shed light on an important aspect of the chemical evolution of the continental crust, the chemical difference between Archean and post-Archean bedrock. The long-standing recognition that Archean continental rocks differ from post-Archean ones is best shown by the marked differences in the rare earth element (REE) pattern of granitoid rocks [cf. *Martin*, 1993, Figure 6]. Archean granitoids are dominated by tonalite-trondhjemite-granodiorite (TTG) assemblages that are characterized by high concentrations of light REE and low concentrations of heavy REE. Post-Archean granitoids, in contrast, have significantly smaller La/Yb ratios due to higher Yb concentrations. Such a contrast in REE pattern is not observed between Archean and post-Archean shales, as Archean shales have La/Yb ratios that are similar to post-Archean granitoids and shales. This observation led *Condie* [1993] to propose that Archean source areas of detrital matter likely contained significantly more basaltic bedrock than is currently observed in the geologic record.

[37] The average bedrock age of present-day continental crust (~475 Myr [*Peucker-Ehrenbrink and Miller*, 2007]) is slightly older than the exorheic portion of the continents (~453 Myr). If the bedrock ages of large-scale drainage regions are weighted according to regional water discharge or suspended sediment flux, average ages are 394 Myr and 336 Myr, respectively. The younger average age of source areas of detrital matter indicates a bias toward young sources. A global analysis of bedrock lithology [*Peucker-Ehrenbrink and Miller*, 2007] indicates that sedimentary and volcanic bedrock are, on average, significantly younger than plutonic and metamorphic bedrock. Together, these observations indicate that young sedimentary and volcanic source regions contribute disproportionately to detrital sediments. As our spatial analysis does not account for the effects of differential weatherability of bedrock, it is likely that the age bias in source areas of runoff and sediment is even larger than indicated by the above estimates, because young sedimentary and volcanic bedrock are more susceptible to erosion that metamorphic and plutonic bedrock. The observed contrast between REE pattern of granitoid rocks and shales in the Archaean may thus simply reflect aliasing of source regions rather than fundamental differences in the abundance of basaltic material in the Archean upper continental crust. We emphasize that the differences in bedrock ages would be even more pronounced if the regional runoff had been weighted according to factors that have been neglected in this study, specifically topographic gradient and regional distribution of rainfall. For instance, *Summerfield and Hulton* [1994] and *Wilkinson and McElroy* [2007] argue that areas of high elevation (i.e., steep topographic gradients) generate disproportionately large quantities of detrital matter. Similarly, our implicit assumption that runoff is generated equally over the entire drainage area introduces an unquantified bias in this study. That these effects can be large and to a significant degree man-made is best illustrated by variations in sediment yields in the Huanghe (Yellow River) drainage basin, where regional yields vary from less than 30 tons km^{-2} yr^{-1} to more than 100,000 t km^{-2} yr^{-1} [*Hassan et al.*, 2008]. Highest denudation rates are concentrated on the Loess Plateau in weakly solidified sedimentary rocks. Future improvements in our approach will need to incorporate such spatial variability.

5. Summary

[38] Two independent lines of evidence indicate that the continental input of Nd to seawater is within uncertainty isotopically identical to the average isotope composition of seawater. This is consistent with the negligible effect submarine hydrothermal Nd inputs have on the Nd budget of seawater. Average bedrock ages of drainage basins correlate with detrital $^{143}Nd/^{144}Nd$ and serve as useful proxies for the dissolved riverine $^{143}Nd/^{144}Nd$. This load is derived preferentially from younger portions of the continental bedrock that is more strongly influenced by volcanic and sedimentary bedrock.

[39] The global riverine runoff of Sr (4.7×10^{10} mol yr^{-1}) has a $^{87}Sr/^{86}Sr$ of 0.7111 that can be interpreted as a 30/70 mixture of Fraser River and Himalaya-like source regions with steep trends of $^{87}Sr/^{86}Sr$ versus bedrock age (weathering-limited), and all other source regions with significantly shallower trends (transport-limited). As we do not yet fully understand the parameters and processes that control the slope of these relationships, it is premature to speculate about the impact of global shifts in slope on the evolution of seawater $^{87}Sr/^{86}Sr$. It is conceivable, however, that temporal variations in the effective slope can lead to changes in seawater

$^{87}Sr/^{86}Sr$ that are not accompanied by changes in the mean bedrock age of the continents.

[40] Finally, we point out that available digital bedrock maps can be utilized in the next generation of models of biogeochemical cycles to parameterize radiogenic isotope compositions in continental runoff [e.g., *Amiotte Suchet and Probst*, 1995; *Amiotte Suchet et al.*, 2003; *Roelandt et al.*, 2010]. It does not seem far fetched to envision models of the temporal evolution of radiogenic isotopes in seawater that combine the use of available paleogeologic maps with paleogeographic reconstructions and global climate models.

[41] **Note added in proof.** *Pattanaik et al.* [2007] report Sr concentrations (μM) and $^{87}Sr/^{86}Sr$ for the Palar (1.71, 0.711636), Ponnaiyar (3.83, 0.716045), Vellar (2.90, 0.711703) and Kaveri (2.69, 0.714978) rivers in India. *Trivedi et al.* [1995] report additional data for the Mahanadi (0.704, 0.7193), Krishna (3.74, 0.7142), Sabarmati (3.36, 0.7177), Mandovi (0.352, 0.7196), Zuari (0.431, 0.7235) and Periyar (0.365, 0.7194) rivers. These data do not significantly change the average values for large-scale drainage region ID 8 (Arabia, India, and SE Asia).

Acknowledgments

[42] We thank the British Columbia Fisheries Service for digital outlines of the Fraser River basin and its tributary basins and the World Resources Institute (WRI, Washington, D. C.) for permission to use raw data for watershed outlines published by *Revenga et al.* [1998]. We benefited from discussion with colleagues at WHOI and the Observatoire Midi-Pyrénées, as well as feedback from colleagues elsewhere, particularly Bruce Wilkinson, Wallace Broecker, Steve Goldstein, Lee Kump, Andy Kurtz, and anonymous reviewers of related NSF proposals. We are grateful for the insightful reviews by Lou Derry and an anonymous reviewer and thank Vincent Salters for the editorial handling of the manuscript. NSF grants EAR-0125873, EAR-0519387, and OCE-0851015 to B.P.-E. and a CNRS-funded "poste rouge" position for B.P.-E. at the Observatoire Midi-Pyrénées in Toulouse supported this work.

References

Albarede, F., A. Vitrac-Michard, J. F. Minster, and G. Michard (1980), Strontium isotopic composition in hydrothermal systems, *Eos Trans. AGU*, *61*(46), 994–995.

Amakawa, H., D. S. Alibo, and Y. Nozaki (2000), Nd isotopic composition and REE pattern in the surface waters of the eastern Indian Ocean and its adjacent seas, *Geochim. Cosmochim. Acta*, *64*, 1715–1727, doi:10.1016/S0016-7037(00)00333-1.

Amakawa, H., D. S. Alibo, and Y. Nozaki (2004a), Nd concentration and isotopic composition distributions in surface waters of northwest Pacific Ocean and its adjacent seas, *Geochem. J.*, *38*, 493–504.

Amakawa, H., Y. Nozaki, D. S. Alibo, J. Zhang, K. Fukugawa, and H. Nagai (2004b), Neodymium isotopic variations in northwest Pacific waters, *Geochim. Cosmochim. Acta*, *68*, 715–727, doi:10.1016/S0016-7037(03)00501-5.

Amiotte Suchet, P., and J.-L. Probst (1995), A global model for present-day atmospheric/soil CO_2 consumption by chemical erosion of continental rocks (GEM-CO_2), *Tellus, Ser. B*, *47*, 273–280, doi:10.1034/j.1600-0889.47.issue1.23.x.

Amiotte Suchet, P., J.-L. Probst, and W. Ludwig (2003), Worldwide distribution of continental rock lithology: Implications for the atmospheric/soil CO_2 uptake by continental weathering and alkalinity river transport to the oceans, *Global Biogeochem. Cycles*, *17*(2), 1038, doi:10.1029/2002GB001891.

Arsouze, T. (2008), Modélisation du cycle océanique du néodyme, Ph.D. thesis, 174 pp., Univ. Toulouse III, Toulouse, France.

Arsouze, T., J.-C. Dutay, F. Lacan, and C. Jeandel (2009), Reconstructing the Nd oceanic cycle using a coupled dynamical-biogechemical model, *Biogeosciences*, *6*, 1–18.

Basu, A., S. B. Jacobsen, R. J. Poreda, C. B. Dowling, and P. K. Aggarwal (2001), Large groundwater strontium flux to the oceans from the Bengal basin and the marine strontium isotope record, *Science*, *293*, 1470–1473, doi:10.1126/science.1060524.

Bertram, C. J., and H. Elderfield (1993), The geochemical balance of the rare earth elements and neodymium isotopes in the oceans, *Geochim. Cosmochim. Acta*, *57*, 1957–1986, doi:10.1016/0016-7037(93)90087-D.

Blum, J. D., and Y. Erel (1995), A silicate weathering mechanism linking increases in marine $^{87}Sr/^{86}Sr$ with global glaciation, *Nature*, *373*, 415–418, doi:10.1038/373415a0.

Bluth, G. J. S., and L. R. Kump (1991), Phanerozoic paleogeology, *Am. J. Sci.*, *291*, 284–308.

Brass, G. W. (1976), The variation of the marine $^{87}Sr/^{86}Sr$ ratio during Phanerozoic time: Interpretation using a flux model, *Geochim. Cosmochim. Acta*, *40*, 721–730, doi:10.1016/0016-7037(76)90025-9.

Cameron, E. M., and K. Hattori (1997), Strontium and neodymium isotope ratios in the Fraser River, British Columbia: A riverine transect across the Cordilleran orogen, *Chem. Geol.*, *137*, 243–253, doi:10.1016/S0009-2541(96)00168-4.

Chao, B. F., Y. H. Wu, and Y. S. Li (2008), Impact of artificial reservoir water impoundment on global sea level, *Science*, *320*, 212–214, doi:10.1126/science.1154580.

Cohen, M. J., C. Henges-Jeck, and G. Castillo-Moreno (2001), A preliminary water balance for the Colorado River delta, 1992–1998, *J. Arid Environ.*, *49*, 35–48, doi:10.1006/jare.2001.0834.

Commission for the Geologic Map of the World (2000), Geologic map of the world at 1:25,000,000, 2nd ed., UNESCO, Paris.

Condie, K. C. (1993), Chemical composition and evolution of the upper continental crust: Contrasting results from surface samples and shales, *Chem. Geol.*, *104*, 1–37, doi:10.1016/0009-2541(93)90140-E.

Dahlqvist, R., P. S. Andersson, and J. Ingri (2005), The concentration and isotopic composition of diffusible Nd in fresh and marine waters, *Earth Planet. Sci. Lett.*, *233*, 9–16, doi:10.1016/j.epsl.2005.02.021.

Dasch, E. J. (1969), Strontium isotopes in weathering profiles, deep-sea sediments, and sedimentary rocks, *Geochim. Cosmochim. Acta*, *33*, 1521–1552, doi:10.1016/0016-7037(69)90153-7.

Davis, A. C., M. J. Bickle, and D. A. H. Teagle (2003), Imbalance in the oceanic strontium budget, *Earth Planet. Sci. Lett.*, *211*, 173–187, doi:10.1016/S0012-821X(03)00191-2.

Douglas, T. A., C. Page Chamberlain, and J. D. Blum (2002), Land use and geologic control on the major elemental and isotopic (δ^{15}N and ^{87}Sr/^{86}Sr) geochemistry of the Connecticut river watershed, USA, *Chem. Geol.*, *189*, 19–34, doi:10.1016/S0009-2541(02)00047-5.

Edmond, J. M. (1992), Himalaya tectonics, weathering processes, and the strontium isotope record in marine limestones, *Science*, *258*, 1594–1597, doi:10.1126/science.258.5088.1594.

Elderfield, H., and J. M. Gieskes (1982), Sr isotopes in interstitial waters of marine sediments from Deep Sea Drilling Project cores, *Nature*, *300*, 493–497, doi:10.1038/300493a0.

Fiege, K., C. A. Miller, L. F. Robinson, R. Figueroa, and B. Peucker-Ehrenbrink (2009), Strontium isotopes in Chilean rivers: The flux of unradiogenic continental Sr to seawater, *Chem. Geol.*, *268*, 337–343, doi:10.1016/j.chemgeo.2009.09.013.

Gaillardet, J., B. Dupré, P. Louvat, and C.-J. Allègre (1999), Global silicate weathering and CO_2 consumption rates deduced from the chemistry of large rivers, *Chem. Geol.*, *159*, 3–30, doi:10.1016/S0009-2541(99)00031-5.

Galy, A., C. France-Lanord, and L. A. Derry (1999), The strontium isotopic budget of Himalayan Rivers in Nepal and Bangladesh, *Geochim. Cosmochim. Acta*, *63*, 1905–1925, doi:10.1016/S0016-7037(99)00081-2.

Goldstein, S. J., and S. B. Jacobsen (1987), The Nd and Sr isotopic systematics of river-water dissolved material: Implications for the sources of Nd and Sr in seawater, *Chem. Geol.*, *66*, 245–272.

Goldstein, S. J., and S. B. Jacobsen (1988), Nd and Sr isotopic systematics of river water suspended material: Implications for crustal evolution, *Earth Planet. Sci. Lett.*, *87*, 249–265, doi:10.1016/0012-821X(88)90013-1.

Goldstein, S. L. (1988), Decoupled evolution of Nd and Sr isotopes in the continental crust and the mantle, *Nature*, *336*, 733–738, doi:10.1038/336733a0.

Graham, S. T., J. S. Famiglietti, and D. R. Maidment (1999), Five-minute, 1/2°, and 1° data sets of continental watersheds and river networks for use in regional and global hydrologic and climate system modeling studies, *Water Resour. Res.*, *35*, 583–587, doi:10.1029/1998WR900068.

Graham, S. T., J. S. Famiglietti, and D. R. Maidment (2000), Five-minute, 1/2°, and 1° data sets of continental watersheds and river networks for use in regional and global hydrologic and climate system modeling studies: Watershed and drainage network data evaluated at three spatial resolutions with supporting documentation, digital data on 5 minute, 1/2 degree and 1 degree resolution, geographic (lat/long) global grids, nine spatial layers with multiple attributes, http://www.ngdc.noaa.gov/ecosys/cdroms/graham/graham/graham.htm, Natl. Geophys. Data Cent., NOAA, Boulder, Colo.

Grosbois, C., P. Négrel, C. Fouillac, and D. Grimaud (2000), Dissolved load of the Loire River: Chemical and isotopic characterization, *Chem. Geol.*, *170*, 179–201, doi:10.1016/S0009-2541(99)00247-8.

Harland, W. B., R. L. Armstrong, A. V. Cox, L. E. Craig, A. G. Smith, and D. G. Smith (1990), *A Geologic Time Scale 1989*, 263 pp., Cambridge Univ. Press, Cambridge, U. K.

Hassan, M. A., M. Church, J. Xu, and Y. Yan (2008), Spatial and temporal variation of sediment yield in the landscape: Example of Huanghe (Yellow River), *Geophys. Res. Lett.*, *35*, L06401, doi:10.1029/2008GL033428.

Henry, F., C. Jeandel, B. Dupre, and J. F. Minster (1994), Particulate and dissolved Nd in the western Mediterranean Sea: Sources, fate and budget, *Mar. Chem.*, *45*, 283–305, doi:10.1016/0304-4203(94)90075-2.

Hicks, M., J. Quinn, and N. Trustrum (2004), Stream sediment load and organic matter, in *Freshwaters of New Zealand*, edited by J. Hardin et al., chap. 12, pp. 12.1–12.15, N. Z. Hydrol. Soc., Wellington.

Hofmann, A. W. (1988), Chemical differentiation of the Earth: The relationship between mantle, continental crust, and oceanic crust, *Earth Planet. Sci. Lett.*, *90*, 297–314, doi:10.1016/0012-821X(88)90132-X.

Jeandel, C. (1993), Concentration and isotopic composition of Nd in the South Atlantic Ocean, *Earth Planet. Sci. Lett.*, *117*, 581–591, doi:10.1016/0012-821X(93)90104-H.

Jeandel, C., D. Thouron, and M. Fieux (1998), Concentrations and isotopic compositions of neodymium in the eastern Indian Ocean and Indonesian straits, *Geochim. Cosmochim. Acta*, *62*, 2597–2607, doi:10.1016/S0016-7037(98)00169-0.

Jeandel, C., T. Arsouze, F. Lacan, P. Téchiné, and J.-C. Dutay (2007), Isotopic Nd compositions and concentrations of the lithogenic inputs into the ocean: A compilation, with an emphasis on the margins, *Chem. Geol.*, *239*, 156–164, doi:10.1016/j.chemgeo.2006.11.013.

Keto, L. S., and S. B. Jacobsen (1988), Nd isotopic variations of Phanerozoic paleoceans, *Earth Planet. Sci. Lett.*, *90*, 395–410, doi:10.1016/0012-821X(88)90138-0.

King, P. B., and H. M. Beikman (1974), Geologic map of the United States, scale 1:2,500,000, U.S. Geol. Surv., Denver, Colo.

Kurz, W. A., C. C. Dymond, G. Stinson, G. J. Pampley, E. T. Neilson, A. L. Carroll, T. Ebata, and L. Safranyik (2008), Mountain pine beetle and forest carbon feedback to climate change, *Nature*, *452*, 987–990, doi:10.1038/nature06777.

Lacan, F., and C. Jeandel (2001), Tracing Papua New Guinea imprint on the central equatorial Pacific Ocean using neodymium isotopic compositions and rare earth element patterns, *Earth Planet. Sci. Lett.*, *186*, 497–512, doi:10.1016/S0012-821X(01)00263-1.

Lacan, F., and C. Jeandel (2004a), Subpolar Mode Water formation traced by neodymium isotopic composition, *Geophys. Res. Lett.*, *31*, L14306, doi:10.1029/2004GL019747.

Lacan, F., and C. Jeandel (2004b), Neodymium isotopic composition and rare earth element concentrations in the deep and intermediate Nordic seas: Constraints on the Iceland Scotland Overflow Water signature, *Geochem. Geophys. Geosyst.*, *5*, Q11006, doi:10.1029/2004GC000742.

Lacan, F., and C. Jeandel (2004c), Denmark Strait water circulation traced by heterogeneity in neodymium isotopic compositions, *Deep Sea Res., Part I*, *51*, 71–82, doi:10.1016/j.dsr.2003.09.006.

Lacan, F., and C. Jeandel (2005a), Neodymium isotopes as a new tool for quantifying exchange fluxes at the continent-ocean interface, *Earth Planet. Sci. Lett.*, *232*, 245–257, doi:10.1016/j.epsl.2005.01.004.

Lacan, F., and C. Jeandel (2005b), Acquisition of the neodymium isotopic composition of the North Atlantic Deep Water, *Geochem. Geophys. Geosyst.*, *6*, Q12008, doi:10.1029/2005GC000956.

Levson, V. M., and T. R. Giles (1995), Glacial dispersal patterns of mineralized bedrock: With examples from the Nechako

Plateau, central British Columbia, *Pap. 1995-2*, 67–76, B. C. Minist. of Energy, Mines, and Pet. Res., Victoria, B. C., Canada.

Lumbers, S. B., and K. D. Card (1991), Chronometric subdivision of the Archean, *Geolog*, *20*(3), 56–57.

Martin, H. (1993), The mechanisms of petrogenesis of the Archaean continental crust—Comparison with modern processes, *Lithos*, *30*, 373–388, doi:10.1016/0024-4937(93)90046-F.

McLennan, S. M. (2001), Relationships between the trace element composition of sedimentary rocks and upper continental crust, *Geochem. Geophys. Geosyst.*, *2*(4), 1021, doi:10.1029/2000GC000109.

Milliman, J. D., C. Rutkowski, and M. Meybeck (1995), River discharge to the sea—A global river index (GLORI), Land-Ocean Interactions in the Coastal Zone (LOICZ) report, 123 pp., R. Neth. Inst. for Sea Res., Den Burg.

Négrel, P., and E. Petelet-Giraud (2005), Strontium isotopes as tracers of groundwater-induced floods: The Somme case study (France), *J. Hydrol.*, *305*, 99–119, doi:10.1016/j.jhydrol.2004.08.031.

Palmer, M. R., and J. M. Edmond (1989), The strontium isotope budget of the modern ocean, *Earth Planet. Sci. Lett.*, *92*, 11–26, doi:10.1016/0012-821X(89)90017-4.

Palmer, M. R., and J. M. Edmond (1992), Controls over the strontium isotope composition of river water, *Geochim. Cosmochim. Acta*, *56*, 2099–2111, doi:10.1016/0016-7037(92)90332-D.

Pattanaik, J. K., S. Balakrishnan, R. Bhutani, and P. Singh (2007), Chemical and strontium isotopic composition of Kaveri, Palar and Ponnaiyar rivers: Significance to weathering of granulites and granitic gneisses of southern Peninsular India, *Curr. Sci.*, *93*, 523–531.

Peucker-Ehrenbrink, B. (2009), Land2Sea database of river drainage basin sizes, annual water discharges, and suspended sediment fluxes, *Geochem. Geophys. Geosyst.*, *10*, Q06014, doi:10.1029/2008GC002356.

Peucker-Ehrenbrink, B., and M. W. Miller (2002), Quantitative bedrock geology of the conterminous United States of America, *Geochem. Geophys. Geosyst.*, *3*(10), 8000, doi:10.1029/2002GC000366.

Peucker-Ehrenbrink, B., and M. W. Miller (2003), Quantitative bedrock geology of Alaska and Canada, *Geochem. Geophys. Geosyst.*, *4*(4), 8005, doi:10.1029/2002GC000449.

Peucker-Ehrenbrink, B., and M. W. Miller (2004), Quantitative bedrock geology of east and Southeast Asia (Brunei, Cambodia, eastern and southeastern China, East Timor, Indonesia, Japan, Laos, Malaysia, Myanmar, North Korea, Papua New Guinea, Philippines, far-eastern Russia, Singapore, South Korea, Taiwan, Thailand, Vietnam), *Geochem. Geophys. Geosyst.*, *5*, Q01B06, doi:10.1029/2003GC000619.

Peucker-Ehrenbrink, B., and M. W. Miller (2007), Quantitative bedrock geology of the continents and large-scale drainage regions, *Geochem. Geophys. Geosyst.*, *8*, Q06009, doi:10.1029/2006GC001544.

Piepgras, D. J., and S. B. Jacobsen (1988), The isotopic composition of neodymium in the North Pacific, *Geochim. Cosmochim. Acta*, *52*, 1373–1381, doi:10.1016/0016-7037(88)90208-6.

Piepgras, D. J., and G. J. Wasserburg (1980), Neodymium isotopic variations in seawater, *Earth Planet. Sci. Lett.*, *50*, 128–138, doi:10.1016/0012-821X(80)90124-7.

Piepgras, D. J., and G. J. Wasserburg (1982), Isotopic composition of neodymium in waters from the Drake Passage, *Science*, *217*, 207–214, doi:10.1126/science.217.4556.207.

Piepgras, D. J., and G. J. Wasserburg (1983), Influence of the Mediterranean outflow on the isotopic composition of neodymium in waters of the North Atlantic, *J. Geophys. Res.*, *88*, 5997–6006, doi:10.1029/JC088iC10p05997.

Piepgras, D. J., and G. J. Wasserburg (1987), Rare earth element transport in the western North Atlantic inferred from Nd isotopic observations, *Geochim. Cosmochim. Acta*, *51*, 1257–1271, doi:10.1016/0016-7037(87)90217-1.

Piepgras, D. J., G. J. Wasserburg, and E. J. Dasch (1979), The isotopic composition of Nd in different ocean masses, *Earth Planet. Sci. Lett.*, *45*, 223–236, doi:10.1016/0012-821X(79)90125-0.

Plank, T., and C. H. Langmuir (1998), The chemical composition of subducting sediments and its consequences for the crust and mantle, *Chem. Geol.*, *145*, 325–394, doi:10.1016/S0009-2541(97)00150-2.

Rai, S. K., and S. K. Singh (2007), Temporal variation in Sr and $^{87}Sr/^{86}Sr$ of the Brahmaputra: Implications for annual fluxes and tracking flash floods through chemical and isotope composition, *Geochem. Geophys. Geosyst.*, *8*, Q08008, doi:10.1029/2007GC001610.

Reeder, S. W., B. Hitchon, and A. A. Levinson (1972), Hydrochemistry of the surface waters of the Mackenzie River drainage basin, Canada—I. Factors controlling the inorganic composition, *Geochim. Cosmochim. Acta*, *36*, 825–865, doi:10.1016/0016-7037(72)90053-1.

Revenga, C., S. Murray, J. Abramovitz, and A. Hammond (1998), *Watersheds of the World: Ecological Value and Vulnerability*, 163 pp., World Resour. Inst., Worldwatch Inst., Washington, D. C.

Roelandt, C., Y. Godderis, M.-P. Bonnet, and F. Sondag (2010), Coupled modelling of biospheric and chemical weathering processes at the continental scale, *Global Biogeochem. Cycles*, doi:10.1029/2008GB003420, in press.

Ronov, A. B. (1989), *Atlas of Lithological-Paleogeographical Maps of the World, Mesozoic and Cenozoic of Continents and Oceans*, 79 pp., Nauk, Saint Petersburg, Russia.

Seyler, P. T., M. Pinelli, and G. R. Boaventura (2003), A first quantitative estimate of trace metal fluxes from Amazon river and its main tributaries, *J. Phys. IV*, *107*, 1213–1218, doi:10.1051/jp4:20030519.

Shaw, D. M., J. J. Cramer, M. D. Higgins, and M. G. Truscott (1986), Composition of the Canadian Precambrian shield and the continental crust of the Earth, in *The Nature of the Lower Continental Crust*, edited by J. D. Dawson, D. A. Carswell, and K. H. Wedepohl, *Geol. Soc. Spec. Publ.*, *24*, 275–282.

Shimizu, H., K. Tachikawa, A. Masuda, and Y. Nozaki (1994), Cerium and neodymium isotope ratios and REE patterns in seawater from the North Pacific Ocean, *Geochim. Cosmochim. Acta*, *58*, 323–333, doi:10.1016/0016-7037(94)90467-7.

Spivack, A. J., and G. J. Wasserburg (1988), Neodymium isotopic composition of the Mediterranean outflow and the eastern North Atlantic, *Geochim. Cosmochim. Acta*, *52*, 2767–2773, doi:10.1016/0016-7037(88)90144-5.

Stallard, R. F., and J. M. Edmond (1983), Geochemistry of the Amazon: 2. The influence of geology and weathering environment on the dissolved load, *J. Geophys. Res.*, *88*, 9671–9688, doi:10.1029/JC088iC14p09671.

Stordal, M. C., and G. J. Wasserburg (1986), Neodymium isotopic study of Baffin Bay water: Sources of REE from very old terranes, *Earth Planet. Sci. Lett.*, *77*, 259–272, doi:10.1016/0012-821X(86)90138-X.

Summerfield, M. A., and N. J. Hulton (1994), Natural controls of fluvial denudation rates in major world drainage basins, *J. Geophys. Res.*, *99*, 13,871–13,883, doi:10.1029/94JB00715.

Syvitski, J. P. M., and A. J. Kettner (2008), Scaling sediment flux across landscapes, in *Sediment Dymanics in Changing Environments: Proceedings of a Symposium Held in Christchurch, New Zealand, December 2008*, *IAHS Publ.*, *325*, 149–156.

Syvitski, J. P. M., C. J. Vörösmarty, A. J. Kettner, and P. Green (2005), Impact of humans on the flux of terrestrial sediment to the global coastal ocean, *Science*, *308*, 376–380, doi:10.1126/science.1109454.

Tachikawa, K., C. Jeandel, and M. Roy-Barman (1999), A new approach to the Nd residence time in the ocean: The role of atmospheric inputs, *Earth Planet. Sci. Lett.*, *170*, 433–446, doi:10.1016/S0012-821X(99)00127-2.

Tachikawa, K., V. Athias, and C. Jeandel (2003), Neodymium budget in the modern ocean and paleo-oceanographic implications, *J. Geophys. Res.*, *108*(C8), 3254, doi:10.1029/1999JC000285.

Tachikawa, K., M. Roy-Barman, A. Michard, D. Thouron, D. Yeghicheyan, and C. Jeandel (2004), Neodymium isotopes in the Mediterranean Sea: Comparison between seawater and sediment signals, *Geochim. Cosmochim. Acta*, *68*, 3095–3106, doi:10.1016/j.gca.2004.01.024.

Trivedi, J. R., K. Pande, S. Krishnaswami, and M. M. Sarin (1995), Sr isotopes in rivers of India and Pakistan: A reconnaissance study, *Curr. Sci.*, *69*, 171–178.

Vance, D., A. E. Scrivner, P. Beney, M. Staubwasser, G. M. Henderson, and N. C. Slowey (2004), The use of foraminifera as a record of the past neodymium isotope composition of seawater, *Paleoceanography*, *19*, PA2009, doi:10.1029/2003PA000957.

Vance, D., D. A. H. Teagle, and G. L. Foster (2009), Variable Quaternary chemical weathering fluxes and imbalances in marine geochemical budgets, *Nature*, *458*, 493–496, doi:10.1038/nature07828.

Wang, H., Z. Yang, Y. Saito, J. P. Liu, and X. Sun (2006), Interannual and seasonal variations of the Huanghe (Yellow River) water discharge over the past 50 years: Connections to impacts from ENSO events and dams, *Global Planet. Change*, *50*, 212–225, doi:10.1016/j.gloplacha.2006.01.005.

Wang, H., Z. Yang, Y. Saito, J. P. Liu, X. Sun, and Y. Wang (2007), Stepwise decrease of the Huanghe (Yellow River) sediment load (1950–2005): Impacts of climate change and human activities, *Global Planet. Change*, *57*, 331–354, doi:10.1016/j.gloplacha.2007.01.003.

Wheeler, J. O., P. F. Hoffman, K. D. Card, A. Davidson, B. V. Stanford, A. V. Okulitch, and W. R. Roest (1997), Geologic map of Canada, *Map D1860A*, version 1.0, scale 1:5,000,000, Nat. Resour. Can., Ottawa, Ont., Canada.

Wilkinson, B. H., and B. J. McElroy (2007), The impact of humans on continental erosion and sedimentation, *Geol. Soc. Am. Bull.*, *119*, 140–156, doi:10.1130/B25899.1.

Wilkinson, B. H., B. J. McElroy, S. E. Kesler, S. E. Peters, and E. D. Rothman (2009), Geologic maps as tectonic speedometers–rates of rock cycling from area-age frequencies, *Geol. Soc. Am. Bull.*, *121*, 760–791, doi:10.1130/B26457.1.